INVESTIGATION OF KINETICS AND THERMOCHEMISTRY OF ION-MOLECULE REACTIONS USING PHOTOIONIZATION MASS SPECTROMETRY

Thesis by

Ashley Deas Williamson

In Partial Fulfillment of the Requirements

For the Degree of

Doctor of Philosophy

California Institute of Technology

Pasadena, California

1976

(Submitted September 17, 1975)

-- to Barbara

ACKNOWLEDGEMENTS

I would like to give credit to many people who have made my years here more rewarding. Primarily I credit my wife Barbara who has shared two of those years, enduring the late nights at the lab and all those discussions of science at parties, and through it all has been a source of inspiration and comfort and been fun to be with besides. I thank Jack Beauchamp for a lot of things in him I hope have rubbed off--not just science facts, but science intuition that allows him to sense new relationships between diverse findings that are often obvious only in retrospect. To Jack I also owe much insight on how to present specialized results in a form comprehensible to a general audience. To the Beauchamp group in particular and to the Caltech community in general I owe many enjoyable hours of serious and trivial discussion. And I owe thanks to my friends at Immanuel Baptist for encouraging me along the way.

Some mention should also be made of those who pay the bills. I gratefully acknowledge the National Science Foundation, the Veterans Administration, and the State of California for helping put me through.

Last but certainly not least, my thanks go to Linda Bryant, Sharon Vedrode, and Joyce Lundstedt for the thankless job of dissertation typing.

ABSTRACT

Chapter I introduces the methodology of photoionization mass spectrometry and lists common applications, including study of ion-molecule reactions. A major advantage of photoionization in the study of ion chemistry lies in the favorable photoionization threshold laws, which frequently permit accurate knowledge of the internal energy distribution of reactant ions. Study of reactions as this distribution is varied allows measurement of the effects of reactant ion internal energy on the reaction kinetics. The photoionization mass spectrometer consists of a discharge lamp, a one-meter normal incidence vacuum monochromator, and a medium pressure quadrupole mass spectrometer. The instrument and its operating conditions are detailed.

Chapter II contains a photoionization study of the reactions of the molecular ion in vinyl fluoride to yield the ionic products $C_3H_3F_2^+$, $C_3H_4F^+$, and $C_3H_5^+$. Quantitative measurements are reported of the effect of the vibrational state of the reactant ion on the product distribution and overall reaction cross section. Reaction cross sections for all three channels decrease with reactant internal energy. The effect on the reaction pathway producing $C_3H_3F_2^+$ is especially pronounced, with 0.19 eV of vibrational excitation being sufficient to reduce the reaction probability by 80%. Deactivation of vibrationally excited reactant ions competes with the reaction and is shown to be an efficient process.

Chapter III details a study of the major ion-molecule reaction pathways in ketene and ketene-d_2 by photoionization mass spectrometry and ion cyclotron resonance spectroscopy. For pro-

cesses involving the molecular ion, the variation of reaction cross section with ion vibrational state is pronounced. The threshold determined for the endothermic process $CH_2CO^+ + CH_2CO \rightarrow C_2H_4^+ + 2CO$ provides a novel confirmation of the recent redetermination of the heat of formation of ketene.

In Chapter IV photoionization efficiency data are presented for the parent and major fragment ions in 2, 2-difluoropropane and 2-fluoropropane. Appearance potentials for CH_3 and CH_4 loss may be used to relate the heats of formation of the olefin radical cations and fluorinated ethyl carbonium ions to the parent neutral and to one another. A thermochemical cycle allows determination of the proton affinities of vinyl fluoride and 1, 1-difluoroethylene. The fragmentation thresholds in 2-fluoropropane appear to be too high by 7-9 kcal/mole. Standard heats of formation determined by this study are: $(CH_3)_2CF_2$, -129.8 ± 3.0 kcal/mole; $CH_3CF_2^+$, 108.5 ± 3.2 kcal/mole; $(CH_3)_2CF^+$, 138.0 ± 1.6 kcal/mole; CH_3CHF^+, 162.6 ± 1.1 kcal/mole.

TABLE OF CONTENTS

CHAPTER I

Introduction and Description of Photoionization Mass Spectrometer

Introduction

This dissertation is a report of research conducted on a medium-pressure mass spectrometer using vacuum ultraviolet photoionization as an ionizing medium. The first chapter will serve as a brief introduction to the technique of photoionization mass spectrometry and description of the design and operation of the instrument used for the present work. Recent results of research performed on this instrument are presented in subsequent chapters.

Photoionization with mass analysis was first reported by Ditchburn and Arnot in 1929.[1] However, serious use of this technique did not become widespread until several decades later, when improved vacuum technology made the spectral region below 2000 Å more easily accessible and allowed for the first time the completely windowless operation necessary for work below the "Li F cutoff" at 1050Å. Since the late 1950's several instruments have been constructed and are in active use, and some informative review articles have been published.[2]

Several aspects of the photoionization process make it a valuable tool for spectroscopic and mass spectrometric studies. To a good approximation, photoionization cross sections obey a step function threshold law, showing an abrupt onset at a photon energy equal to the ionization potential of the species studied and showing only slow variation with photon energy above this threshold. In many molecules the thresholds for higher energy states of the ion behave similarly. In those cases the photoionization efficiency (defined as ions formed per incident photon) has a steplike structure and since the step heights are proportional to the number of ions formed in the corresponding states,

the distribution of internal energy states may be determined. Other types of ionization processes occur which show different threshold behavior and may also be studied by photoionization mass spectrometry. Most neutral systems have excited states which lie above the first ionization potential. In addition to more general modes of decay such as fluorescence or dissociation, these states occasionally cross dissociative ionic levels yielding a positive-negative ion pair.[3] Frequently such "superexcited" states mix with the ionization continuum and autoionize.[4] They then appear as resonances in the ionization efficiency curve.

Because of its favorable threshold behavior and the inherent high energy resolution of optical techniques, photoionization mass spectrometry is a versatile technique which has found diverse uses. A common application is the gathering of accurate thermochemical data, since ionization and appearance potentials may be determined using dispersed light with much better accuracy than available with nonspectroscopic techniques. Analytical applications of photoionization typically involve use of the high energy resolution available to selectively ionize minor components in a mixture.[5,6] An early application was to test statistical theories of mass spectral decomposition by comparison with detailed data on fragmentation patterns.[7]

A relatively new application of photoionization mass spectrometry is the study of ion-molecule reactions. Much of the work in this field has been performed by W. A. Chupka, who has written an extensive and informative review article on the subject.[8] The power of photoionization for the study of ion reactions lies in the fact that

ions can frequently be prepared in known distributions of internal states, as mentioned above. By varying the population of internal states, the effect of internal energy on reaction cross sections can be measured. Frequently these data have significance in understanding reaction mechanisms (see Chapter III).

This dissertation describes investigations performed in our laboratory of the dynamics and thermochemistry of ion-molecule reactions. The primary technique in these studies is photoionization mass spectrometry, with ancillary studies performed by ion cyclotron resonance (ICR) spectrometry. In the latter part of this chapter, the details and operating procedures of the Caltech-JPL photoionization mass spectrometer are described. Chapter II describes investigations of the effect of vibrational energy on the reactions of the molecular ion in vinyl fluoride. Dramatic effects on both the reaction rate and product distributions are described. Chapter III details the investigation of ion-molecule reactions in ketene, where both exothermic and endothermic pathways exist. Chapter IV describes use of appearance potentials from dissociative ionization to calculate the gas phase proton affinities of vinyl fluoride and 1,1 difluoroethylene.

Published work related to the present investigations of ion-molecule reaction dynamics include studies of the effect of vibrational and electronic excitation on the reactivity of the parent ion in ethylene,[9] the effect of vibrational energy in the reaction of acetylene molecular ions with H_2,[10] and study of the effect of metastable electronic excitation on the reaction of O_2^+ ($a\,^4\Pi_u$) with H_2.[11] In addition, unpublished photoionization studies have been made of the reactions

of $NO^+(v = 0 - 4)$ with organic molecules, previously studied by ICR methods.[12] Other photoionization studies include ionization efficiency measurements in trans-azomethane[13] and determination of the heat of formation of the allyl cation.[14]

Description of Instrument

A block diagram of the photoionization instrument is shown in Fig. 1. In operation, vacuum ultraviolet radiation is formed in a discharge in the lamp. Passing into a concave grating vacuum monochromator, it is dispersed and focussed into the ion source of the mass spectrometer region of the instrument, where the photon flux is detected. In the source the light encounters gaseous samples and forms photoions which may at higher pressures react with neutral species there. Both primary and reaction product ions are extracted upwards through a quadrupole mass filter and detected by an electron multiplier. The system is completely windowless; that is, there are no obstructions in the path of the light or ion beams. In order to maintain the required pressure differentials, extensive pumping is required. Each of these component systems will be described in detail, as will the ancillary electronics and operating procedures.

A. Light Sources

The lamp configuration currently in use is displayed in Fig. 2. The lamp itself is a McPherson Model 630 Hinterrigger style discharge lamp, consisting of an air-cooled, aluminum cathode supported by three ceramic posts, a water-cooled capillary, and a water-cooled aluminum cathode. Our lamp was modified from the McPherson

Figure 1. Schematic diagram of photoionization mass spectrometer. Major components are labelled in the figure.

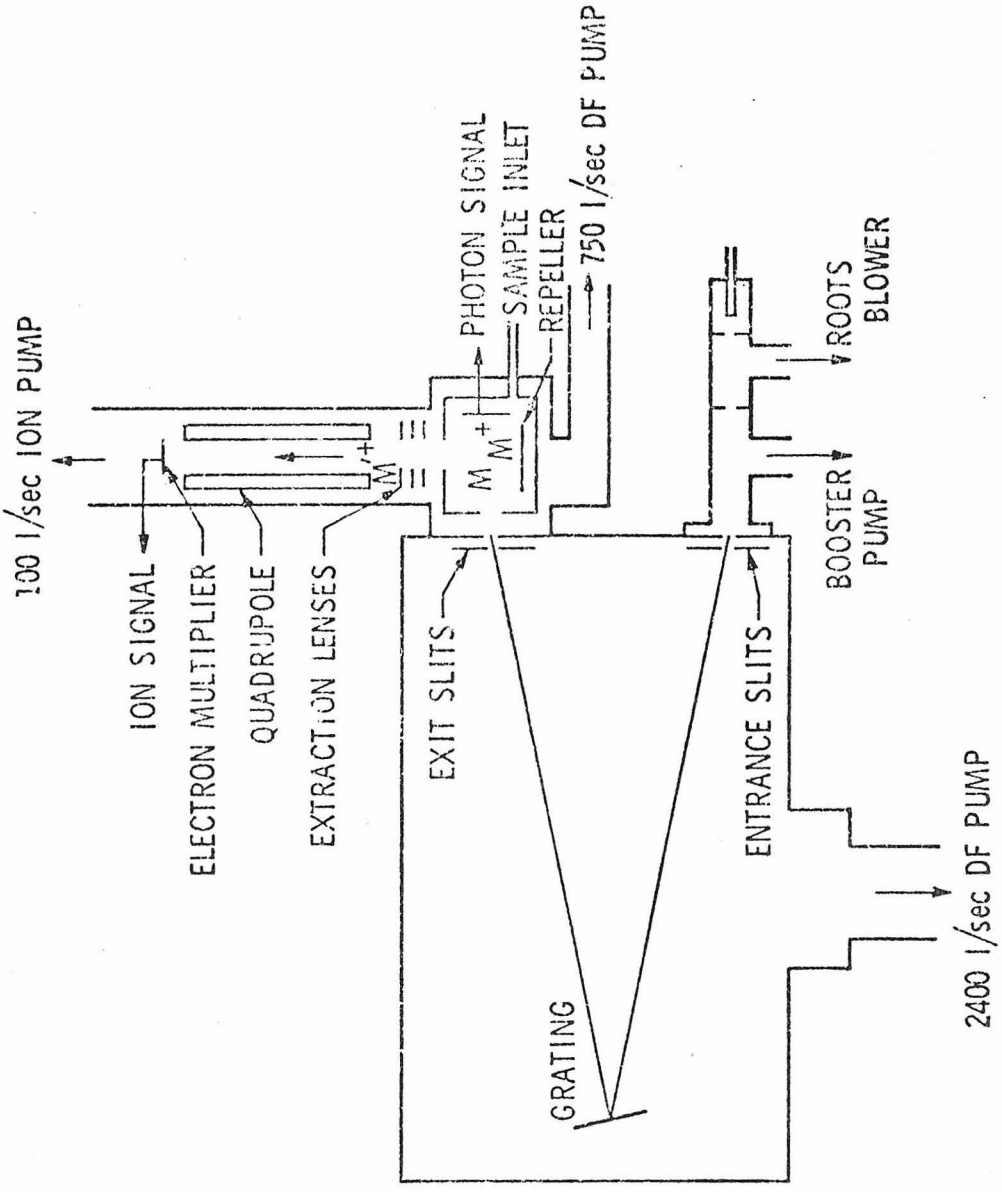
100 l/sec ION PUMP
ION SIGNAL
ELECTRON MULTIPLIER
QUADRUPOLE
EXTRACTION LENSES
EXIT SLITS
GRATING
PHOTON SIGNAL
SAMPLE INLET
REPELLER
750 l/sec DF PUMP
ENTRANCE SLITS
BOOSTER PUMP
ROOTS BLOWER
2400 l/sec DF PUMP

Figure 2. Hinterregger-type discharge lamp. C - cathode, Cp - quartz capillary, A - anode.

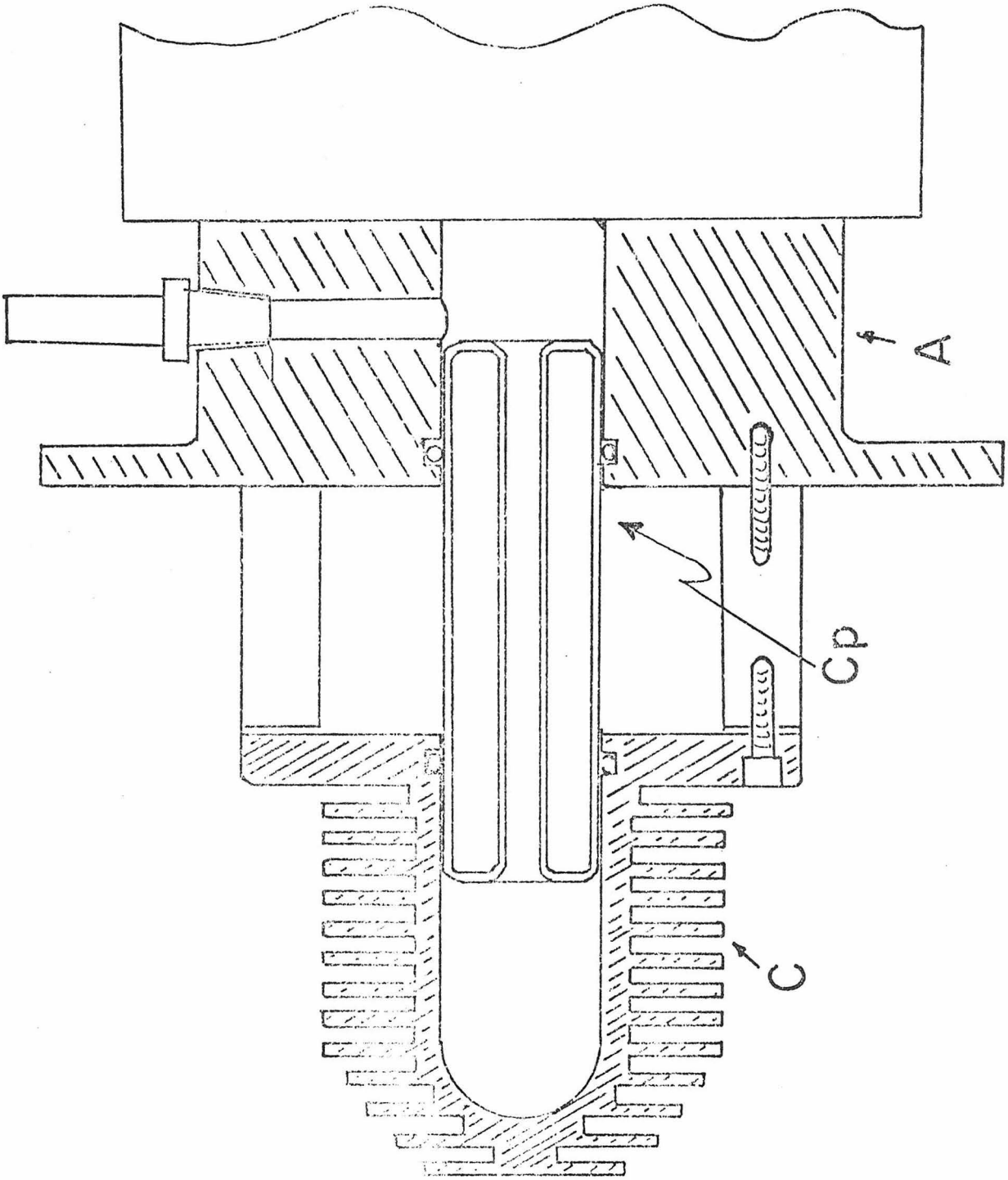
A
Cp
C

design by electrically isolating the anode from ground by a plexiglass spacer, and by changing the lamp gas inlet configuration. Gas is admitted between the monochromator and the lamp anode. Part of the gas flows through the first differential pumping slit and part through the lamp, where it is pumped away through an insulated line connected to the cathode. Both modifications were added in an attempt to eliminate high voltage arcs to the differential pumping slit which damage the slit and generate noise due to electromagnetic interference in the electronics. Arcs remain a problem when the lamp is run in a dc mode, but can be controlled by varying the pressure of the lamp gas and running at lower lamp currents (250 ma.). This configuration also minimizes the tendency of bits of aluminum from the cathode to be sputtered off and into the slit assembly, obstructing the light path.

Some work was also performed using the "pi" lamp of Huffman, et al.,[15] but this source was abandoned due to several difficulties. It was less compact, thus giving rise to problems maintaining optical alignment as well as danger of leakage or of shock from exposed high voltage. Worse yet, the electrodes tended to melt if the lamp pressure became too low. The only advantage of this configuration was the absence of electrical arcing problems.

The two emission spectra used for these studies were the many line spectrum of molecular hydrogen extending from 900 - 1600 Å (7.7 - 13.8 eV) and the Hopfield continuum in helium from 600 - 1000 Å (12.4 - 20.6 eV). Both excitation spectra are adequately discussed in an excellent text by Samson[16] on vacuum UV spectroscopy, so only the details relevant to our system will be discussed.

The hydrogen line spectrum is excited by a dc discharge in roughly 1 torr of hydrogen. Typical operating currents are 250 - 500 ma., which require voltages of 800 - 1200 V with a 400 Ω series resistor for ballast. Wavelengths of isolated lines may be assigned to an accuracy of 0.1 Å using a photoelectric atlas of the spectrum.[17]

The Hopfield continuum is excited using a thyratron-switched pulsed high voltage supply after the design of Huffman, et al.[18] Optimum parameters were found to be 100 kHz repetition rate, about 1 μsec pulse width, 10 kV (or as close as possible), and as high an instantaneous current obtainable without damage to the thyratron (the current could be controlled by varying the storage capacitor in the power supply). Due to power supply difficulties we were forced to operate at 1 kHz and 3 kV. The pulsed circuit is subject to causing electrical interference which affected several pieces of electronic gear (in particular the monochromator drive servo system) so scrupulous attention to shielding was necessary. Typical helium pressures are 60 torr. The light intensity of strong lines in the hydrogen spectrum is found to be an order of magnitude greater than that of the maximum of the helium continuum, consistent with the reported relative heights of the two excitation sources.[16]

In order to purify the lamp gases, a glass gas-handling system was constructed with two traps filled with Linde 13 X molecular sieve which could be cooled with liquid nitrogen. The spectra were found to be relatively insensitive to the use of the traps, and since the glass gas line was subject to breakage and leaks at the glass to metal junctions, the present design is not recommended for future use.

B. Vacuum Monochromator

In our instrument light from the discharge lamp is dispersed by a McPherson model 225 vacuum monochromator. The monochromator is a one meter instrument of McPherson type near-normal incidence design which has low astigmatism and is capable of a reciprocal dispersion of 8.3 Å/mm when equipped with gratings with 1200 grooves/mm. The monochromator is equipped with fixed entrance slits of 10, 50 and 100 μm; the exit slit is variable from 5 to 2000 μm. Valves exist to isolate the monochromator from both slit assemblies.

Two 1200 line/mm replica gratings have been used in our instrument. One is a MgF_2 coated aluminum grating blazed for 1200 Å in first order. This grating has high (~ 60%) reflectivity above 1200 Å but the reflectivity deteriorates rapidly with decreasing wavelength due to absorption. The second grating is gold coated and has better reflectance at short wavelengths. It is blazed for 800 Å in first order, making it more useful for studies below 1000 Å (above 12.4 eV). This grating has been left installed in the instrument. When changing gratings, the Rowland circle was aligned using a He-Ne laser to adjust the slit image in zero order (direct reflection). Then the radial displacement of the grating path was adjusted using a mercury penray lamp in first order with a photomultiplier detector. The adjustment procedure is outlined in the manual for the monochromator.

The monochromator is equipped with a motor drive for the grating. However, in order to achieve better wavelength precision and reproducibility an external servo system was purchased from Theta

Instrument Corp. The Theta Decitrak servo system consists of a Slo-Syn HS-25 stepping motor mounted externally on the gear box of the grating drive and an optical encoder mounted inside the vacuum system, coupled directly to the worm gear of the grating drive shaft where minimal backlash is expected. The associated electronics contain digital and analog outputs indicative of the grating position, with an accuracy in position of 0.1 Å.

C. Mass Spectrometer Region

Light emerging from the monochromator exit slit enters the mass spectrometer region of the instrument. This region, shown in Fig. 3, contains the ion source, photon flux detector, electrostatic lenses and the quadropole mass filter, and electron multiplier ion detector. Each of these components will be described in detail.

A sketch of the ion source is displayed in Fig. 4. It is an enclosed box designed to be mounted as close as mechanically feasible to the monochromator exit slit. The dimensions of the box are such that the diverging photon beam does not contact its sides, top or bottom. Apertures in the source are kept to a minimal area so that higher pressures can be used for study of reactions. The photon entrance slit measures 0.125 x 0.407 in.; the ion exit hole has 0.125" diameter. There is a small hole associated with a filament electron beam source which can be used as an alternate ionizing agent. The net conductance of all three apertures was measured to be 3.4 ℓ/sec at pressures typical of normal operation. In the bottom of the source is a U-shaped repeller used to extract ions from the source region. The focussing properties of this repeller are not perfect, as indicated

Figure 3. Mass spectrometer region of photoionization mass spectrometer. I - ionization chamber, L - electrostatic lens system, Q - quadrupole mass filter, EM - channel electron multiplier, P - pumping stack.

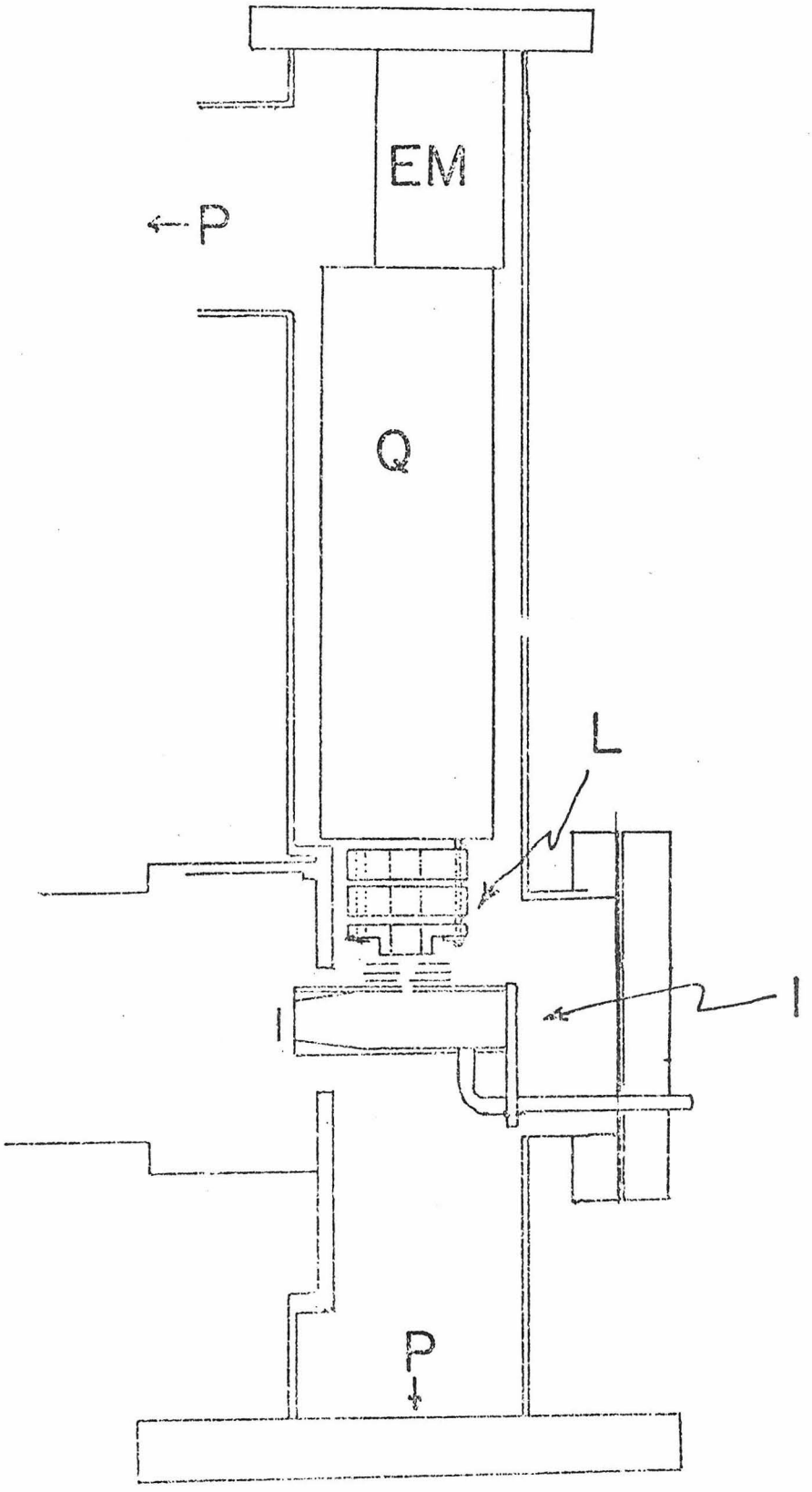
EM
P
Q
L
I
I
P

Figure 4. Ionization source region of photoionization mass spectrometer. Apertures are kept small so that pressures of $\sim 5 \times 10^{-3}$ torr can be obtained without sacrificing high vacuum in mass filter.

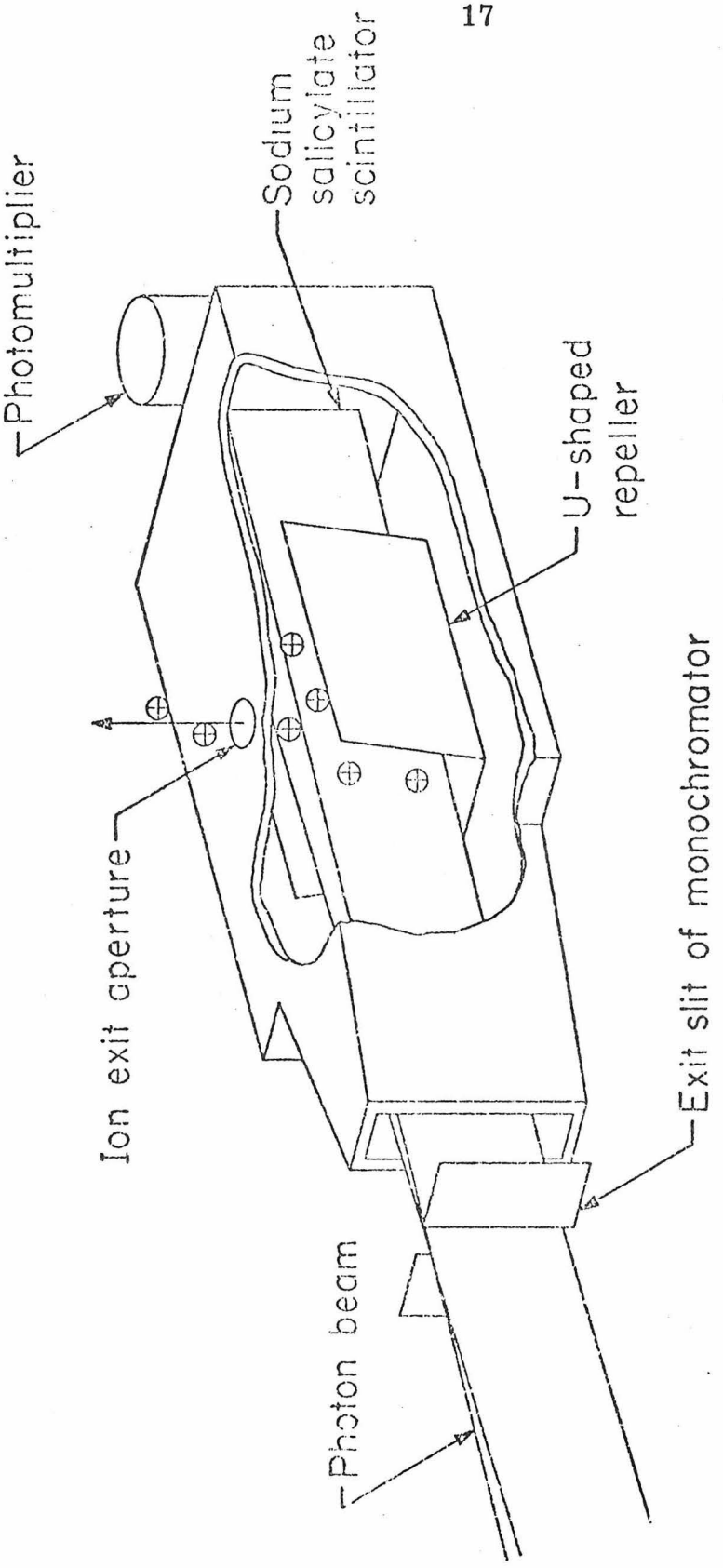
Photomultiplier
Sodium salicylate scintillator
U-shaped repeller
Ion exit aperture
Exit slit of monochromator
Photon beam

by the fact that the maximum ion signals are obtained with the repeller biased in the range of -0.01 to +0.20 V with respect to the source region. These settings are typically used, with the advantage that the resulting low kinetic energies allow increased residence times and thus higher reaction conversions for a given pressure.

Sample pressures are measured with an MKS Baratron capacitance manometer with a model 90H1 preamplifier-head assembly. Typical pressures ranged from 0.01 to 5 millitorr.

The source region also contains the photon flux detector. At present light intensity is measured by a sodium salicylate-photomultiplier combination. The use of sodium salicylate as a phosphor has been described in detail by Samson.[16] In the present configuration the back wall of the ion source contains a salicylate-coated glass window. Behind the window is a small blue-sensitive photomultiplier (RCA model 8571) mounted in a copper block. The block is connected by a braid of OFHC copper to a liquid nitrogen-cooled reservoir outside the vacuum chamber. The steady-state temperature of the photomultiplier block is -26 °C; at this temperature dark current is roughly 5×10^{-11} amps, comparable to the smallest signal levels encountered. The voltage specifications for the photomultiplier are 800 V typical, 1000 V maximum recommended for operation. We have found that operation at a reduced voltage of 550 V gives optimum signal to noise for our experimental conditions. The photo tube has the advantage of high output current and relatively constant sensitivity over the entire range of photon energies used on our instrument. It has one major disadvantage. As mentioned by Samson,[16] the quantum efficiency

of sodium salicylate varies somewhat between 900 Å and 1600 Å, and this variation may become pronounced after aging and exposure to some chemicals. Thus, one salicylate coating on our instrument was found to vary by a factor of 2 between 1160 Å and 1000 Å. For this reason corrections for fluorescence yield have to be made when the precise shape of photoionization efficiency curves is important. These corrections are best made by comparing measured photoionization efficiency curves with absolute cross section measurements where they exist. Useful absolute measurements exist for NO from 1340 to 580 Å[19], acetone, propylene, ethylene and acetylene from their ionization potentials to 1050 Å[20], and the rare gases above their ionization potentials.[21] The advantage of these systems is that the relative photoionization cross sections of these measurements are quite reliable also.

An alternate photon detector formerly used with our system was a platinum photocathode assembly mounted inside the ion source. Photoelectron loss from the grounded platinum foil assembly gave rise to currents on the order of 10^{-13} amps under typical operating light fluxes. Photocurrent from this source was measured by a Cary 401 vibrating reed electrometer, as is output current for the present phosphor-photomultiplier system. A positively biased copper anode in the form of a ring was supposed to collect the photoejected electrons. This system had several disadvantages, some inherent and some due to design errors. The photocurrents were smaller by three to four orders of magnitude than the present system, and the photoelectric yield of platinum becomes vanishingly small for wavelengths greater

than about 1400 Å. A significant fraction of the photoelectrons were not collected by the anode but rather accelerated into the ionization region where they caused an unwelcome background due to electron impact ionization. Even more seriously, the fields due to the photon detector deflected photoions in the source, causing a decrease in detection efficiency and adding several volts of kinetic energy to the ions. This effect interfered with the study of ion-molecule reactions.

For some applications a photocathode assembly has advantages, particularly if precautions are taken to isolate the detector electrically from the ionization region. The photoelectric yield of metals like platinum is not as subject to aging or poisoning as the quantum yield of sodium salicylate, nor is it likely to change rapidly in a small spectral region like poisoned salicylate. Second, the photocathode is insensitive to visible light, so is useful where light emission arises from other parts of an experiment, such as ovens or discharge sources.[22]

Ions formed in the source and ejected by the repeller field encounter two sets of three lenses each, designed to focus the ions into the mass filter. Three lenses 0.020" thick and spaced 0.125" apart are attached to the ion source. The second set 0.500" thick and spaced 0.125" apart, are attached to the outer case of the mass filter. Typical operating voltages for positive ions are: ion source, + 7.00 V, thin lens 1, 0V; thin lens 2, -39V; thin lens 3, -100V; thick lens 1, -23V; thick lens 2, -67V; thick lens 3, -10V; quadrupole assembly-grounded.

The quadrupole mass filter is a flange mounted Extranuclear model 324-9 with 3/4 inch cylindrical rods. When operated with the

D1 or D2 heads, the instrument has high transmission and modest resolution (resolution of adjacent masses to 10% of peak height can be achieved in the usable mass range below 200 amu.). Typically the maximum mass limit of 250 amu is sufficient for the systems studied.

Like many quadrupole controllers, the Extranuclear model QPS power supply is resistance programmed. This feature allowed external mass selection by switching preset potentiometers in series with the panel "manual mass" control. In the present system of operating, this switching is performed by a programmable controller described later.

Mass selected ions are detected by a Bendix Channeltron model 4501 operated in pulse counting mode. Output pulses are amplified by a wide band preamplifier and fed into a Hewlett-Packard Model 5243 counter operated in ratio mode. The Schmidt trigger in the input amplifier of the counter serves as a lower level discriminator for the ion signal. The ion signal is counted for a period inversely proportional to the photon flux, using the following method. The output current of the electrometer which measures the photon signal is fed to an active filter and then to a voltage to frequency converter. Ions are counted for a preset number of counts from the voltage-to-frequency converter. This method assures that ions are observed over the same integrated photon flux even though the exciting spectrum may vary dramatically in intensity. Typical count times range from 1 to 200 sec. for each wavelength depending on the intensity of the photon beam and of the ion signal. The output of the counter is fed into a digital printer, which makes a permanent copy of the number of counts and the wave-

length setting.

D. Vacuum System

As was mentioned above, the pumping requirements of our system are severe due to the necessity to maintain high and low pressures in adjacent regions with no separating windows. The most stringent requirements occur in the discharge source. The lamp is operated at 1 to 80 torr; the monochromator should be kept on the order of 10^{-5} torr. There are two factors in the pressure specifications of the monochromator. First, absorption must be minimized, which is not a large problem with H_2 and He which are highly transparent in the regions of their spectra. More important, the vacuum must be extremely clean. Traces of organic materials can be adsorbed on the grating where they are quickly decomposed by the high intensity vacuum UV light to form deposits, resulting in low reflectivity and high scattered light. In order to maintain the necessary high pressure differential between the lamp and monochromator, two stages of differential pumping are employed. The monochromator entrance slit serves as the barrier between the lamp and the first differential pumping region which is evacuated by a 350 cfm. Leybold-Heraeus Roots blower pump backed by a 53 cfm rotary vane pump. The second differential pumping region, separated by a 0.072" x 0.196" opening designed not to impede the optical path, is evacuated by an 800 ℓ/sec NRC-6 six inch oil diffusion pump with a liquid nitrogen-cooled baffle and backed by a 50 cfm Welch model 1398 mechanical pump. A third aperture with dimensions 0.138" x 0.230" separates

this region from the monochromator, which is pumped by an NRC VHS-6 six inch oil diffusion pump with a rated pumping speed of 750 ℓ/sec (trapped). With this pumping configuration, the lamp may be operated with 70 torr of helium and a 50 μ entrance slit, and the pressure in the monochromator can be maintained at 4×10^{-5} torr. In the mass spectrometer region it is desirable to have high sample pressures in the ion source but necessary to maintain pressures less than 10^{-5} torr in the mass filter and at the electron multiplier. This is accomplished primarily by a 700 ℓ/sec CVC four inch oil diffusion pump and the low conductance of the source with its small apertures. There is an additional pumping stack near the electron multiplier leading to a 100 ℓ/sec ion pump. This pump does not bear the greater part of the pumping load during normal operation and is normally turned off due to ions ejected from the pump which cause stray counts by the electron multiplier. However the ion pump may be left on continuously to maintain a clean vacuum in the mass spectrometer when the instrument is not in use.

Operating Procedure

The measurements most frequently made with the present instrument are photoionization efficiency curves, plots of ion signal divided by photon flux over a range of photon energy. Since the efficiency curves for several ions may be desired, it is necessary to be able to observe several masses over a large wavelength range. In order to assist in data collection, a small programmable controller was constructed which automates several of the instrumental functions.

The controller has 10 selectable potentiometers which may be set and then switched in series with the programming potentiometer of the mass filter power supply. The potentiometers are switched into the circuit by a stepping relay, which may advance either by push-button command or automatic control. When automatic switching is desired, the step command is taken from the point cycle of the ratio counter-printer circuit. Thus, when activated, the controller will sequence through the potentiometers selected, taking data for each mass, printing it on digital tape, and advancing to the next mass until each mass has been observed. The operator then changes the wavelength using the Decitrak servo system, restarts the cycle and the data collection continues.

For operation with the hydrogen spectrum, there is little more involved than selecting wavelengths using a spectral atlas,[17] adjusting the monochromator from the Decitrak console, starting the controller cycle, and collecting the printout. Things are slightly different with the Hopfield continuum. Due to the high power of the excitation pulse of this spectrum, electromagnetic interference is induced in the detector preamplifier circuit during the pulse. Since the ions do not arrive until $\sim$ 70 μsec later, gating the counter off except in a window 50 - 500 μsec after the power supply pulse clearly eliminates the interference from the ion signal. However, since the counter cannot be gated while in ratio mode, the ion signal must be detected in the manual count mode, counting for a fixed time period, and the photon signal detected in the same manner using a second counter. The two signals then are recorded and their ratio

taken later in the data analysis. The gating signal is fed into the external time base of the counter.

Photoionization efficiency data may be collected for the molecular ion of a molecule, yielding the first and higher ionization potentials and Franck-Condon factors and allowing study of autoionization phenomena. In addition, photoionization efficiencies may be measured of fragment ions, allowing measurement of appearance potentials and study of fragmentation kinetics or ion-pair processes. Finally, at higher pressures photoionization efficiencies may be taken for ion-molecule reaction products. There are basic considerations common to all of these measurements, although more critical with the weaker signals like those from weak fragments or reaction products. The experimental factors which may complicate any of these measurements are slow drift in the pressure or quadrupole setting, scattered light, and varying efficiency of the photon detector.

Drift in either pressure or the quadrupole often occurs, even though the stability of both the sample inlet leak valve and the mass filter are high. In order to correct for this, all photoionization efficiency signals are measured relative to the signal at a fixed reference wavelength. This signal is measured at intervals depending on how critical the accuracy of the measured intensities is, and a long term correction for instrumental drift is developed and applied to the data. Selection of the reference wavelength is arbitrary, but experience suggests certain criteria. Since high statistical accuracy is desired, a reference wavelength should be a point of relatively high photon flux and of relatively high ion signal for each ion for which corrections will

be made. It should not occur in a spectral region where the photoionization efficiency is rapidly varying unless a well-isolated spectral line is used. It is also convenient if the reference wavelength lies within the relevant spectral region of the ions being studied.

A second complication is scattered light of energy higher than that selected by the monochromator. Usually, this is no problem, since scattered light rarely if ever exceeds 1% of the total light in even a weak spectral region so it cannot be detected by intensity measurements. The occasions when scattered light causes complications arise when it is necessary to measure a weak signal for an ion that is formed in abundance in a higher energy spectral region. Examples of such situations are ionization potential measurements when the Franck-Condon overlap for the adiabatic ionization potential is very small, measurements at wavelengths where the intensity of dispersed light is very small, and measurements of ionization efficiencies for ions from ion-pair processes or ion-molecule reactions (or for free radical species) in which an abundant fragment ion occurs at the same mass but higher energies. The background due to scattered light is approximately constant, but for a line spectrum varies in proportion to the wavelength selected light. Under conditions where only the scattered light component is important (such as well below the threshold of the desired process) the scattered light contribution will be proportional to count time and thus inversely proportional to the intensity of the transmitted photon beam when ratio counting is used. This allows development of a constant of proportionality to be used for correcting wanted ion signals for scattered light. As

mentioned above, such corrections are usually negligible and thus not used.

The third possible complication is that of accounting for the changing efficiency of the photon detector. Such corrections have been described for the photomultiplier-phosphor detector and the adaptation of this technique to other photon detectors is the same in principle. It is important to note that these corrections are quite important for the study of ion molecule reactions where the assumption of step function behavior is made. Any uncertainty in the relative photoionization efficiency as the wavelength is scanned causes proportional uncertainty on the population of interval states measured. Likewise pressure drift in particular is important where the reactions of an ion with its parent neutral are studied, since the product ion will have second order dependence on pressure rather than linear.

The preceding paragraphs contain provisions for correction of systematic errors to which the system is liable. In many cases, no correction or calibration for any of these factors is necessary. However, these effects should be taken into consideration when they are likely to be important.

In addition to photoionization efficiency measurements, two other experiments are occasionally useful when studying ion-molecule reactions. The first is observation of relative ionic abundances as a function of pressure to extract kinetic data. Since the residence time in our ion source is not well characterized, the absolute accuracy of measured reaction rate constants is not expected to be as high as can be obtained by other techniques. However, relative reaction

rates measured for different wavelengths may be instructive,[10] and the kinetics of deactivation of excited ionic states can occasionally be measured (Ref. 9 and Chapter II).

The second technique which has been used to study ion-molecule reactions is the observation of fractional ionic abundances as a function of time in a pulsed experiment. In this technique, the light source is driven by the pulsed power supply (the hydrogen spectrum can be excited in a pulsed mode by this technique). The ion repeller is placed at the same nominal potential as the ion source, so that ions formed emerge through quasi-thermal diffusion. The intensity of each ion is accumulated for a suitable period in a multichannel analyzer with 10 μsec dwell time per channel. The ion signals are then corrected for residence time and flight time in the mass spectrometer and normalized. Excellent agreement with published rates has been obtained for systems in which the parent and product ions do not differ greatly in mass.

Acknowledgements and Collaborators

The Caltech-JPL photoionization mass spectrometer has been funded by California Institute of Technology through grants by the President's Fund. Funds have in addition been received from the Energy Research and Development Agency, and support from the National Aeronautics and Space Administration, including the use of Jet Propulsion Laboratory facilities, is also acknowledged. Part of the purpose of this instrument was to encourage collaborative efforts involving Caltech and JPL personnel. This goal has been achieved in the performance of a number of studies, some still unpublished,

involving workers of these institutions and from outside. Collaborators include Ashley D. Williamson, Pierre R. LeBreton, J. L. Beauchamp, Michael S. Foster, and Reed R. Corderman (California Institute of Technology), Wesley T. Huntress, Joseph M. Ajello, Arthur L. Lane, and Kevin Monahan (Jet Propulsion Lab), S. E. Buttrill (U. of Minnesota), and Michael T. Bowers, Donald Aue, Walter Chesnavich, and William Davidson (U. of California, Santa Barbara). A bibliography of publications performed on the photoionization mass spectrometer is given as an appendix to this chapter.

Bibliography of Published Work Using Caltech-JPL Photoionization Mass Spectrometer

Formation of HO_2^+ by Reaction of Metastable O_2^+ Ions with H_2

J. M. Ajello, W. T. Huntress, A. L. Lane, P. R. LeBreton, and A. D. Williamson, J. Chem. Phys., 60, 1211 (1974).

Photoionization and Ion Cyclotron Resonance Studies of the Reaction of Vibrationally Excited $C_2H_2^+$ Ions with H_2

S. E. Buttrill, Jr., J. K. Kim, W. T. Huntress, Jr., P. LeBreton, and A. Williamson, J. Chem. Phys., 61, 2122 (1974).

Photoionization and Ion Cyclotron Resonance Studies of the Reaction $C_2H_4^+ + C_2H_4 \rightarrow C_3H_5^+ + CH_3$

P. R. LeBreton, A. D. Williamson, and J. L. Beauchamp, J. Chem. Phys., 65, 1623 (1975).

Photoionization Mass Spectrometry of trans-Azomethane

Michael S. Foster, Ashley D. Williamson, and J. L. Beauchamp, Int. J. Mass Spectrom. and Ion Phys., 15, 429 (1975).

Photoionization Measurement of the Heat of Formation of Allyl Cations

S. E. Buttrill, Jr., A. D. Williamson, and P. LeBreton, J. Chem. Phys., 62, 1586 (1975).

Cross-Section for the Dissociative Photoionization of Hydrogen by 584 Å Radiation: The Formation of Protons in the Jovian Ionosphere

K. M. Monahan, W. T. Huntress, A. L. Lane, J. M. Ajello, T. E. Burke, P. R. LeBreton, and A. Williamson, Planet. Space Sci., 22, 143 (1974).

Time-Resolved Photoionization Mass Spectrometry. Unimolecular Fragmentation of Toluene Molecular Ions Near Threshold

S. E. Buttrill, J. Chem. Phys., 61, 619 (1974).

Formation of O_3^+ by the Reaction of Metastable O_2^+ Ions with O_2

J. M. Ajello, K. D. Pang, and K. M. Monahan, J. Chem. Phys., 61, 3152 (1974).

Production of N_2O^+ by Reaction of Metastable O_2^+ Ions with N_2

J. M. Ajello and P. Rayermann, J. Chem. Phys., 62, 2917 (1975).

A Photoionization Study of the Formation of CO_2^+ by the Reaction of Excited O_2^+ Ions with CO

J. M. Ajello, J. Chem. Phys., 62, 1863 (1975).

References

1. R. W. Ditchburn and F. L. Arnot, Proc. Roy. Soc., A123, 516 (1929).
2. N. W. Reid, Int. J. Mass Spectrom. Ion Phys., 6, 1 (1971); and Refs. 3a - n contained therein are the most comprehensive reviews, though somewhat dated.
3. V. H. Dibeler and J. A. Walker, J. Chem. Phys., 43, 1842 (1965).
4. U. Fano, Phys. Rev. 124, 1866 (1961).
5. W. Poschermeder and P. Warneck, J. Appl. Phys., 37, 2812 (1972).
6. R. Atkinson, B. J. Finlayson, and J. N. Pitts, J. Amer. Chem. Soc., 95, 7592 (1973).
7. W. A. Chupka and J. Berkowitz, J. Chem. Phys., 47, 2921 (1967).
8. W. A. Chupka, "Ion-Molecule Reactions by Photoionization Techniques" in Ion Molecule Reactions, ed. J. L. Franklin (Plenum, N.Y., 1972).
9. P. R. LeBreton, A. D. Williamson, J. L. Beauchamp and W. T. Huntress, J. Chem. Phys., 65, 1623 (1975).
10. S. E. Buttrill, Jr., J. K. Kim, W. T. Huntress, Jr., P. LeBreton, and A. Williamson, J. Chem. Phys., 61, 2122 (1974).
11. J. M. Ajello, W. T. Huntress, A. L. Lane, P. R. LeBreton, and A. D. Williamson, J. Chem. Phys., 60, 1211 (1974).
12. A. D. Williamson and J. L. Beauchamp, J. Amer. Chem. Soc., 97, 0000 (1975).
13. Michael S. Foster, Ashley D. Williamson, and J. L. Beauchamp, Int. J. Mass Spectrom. Ion Phys., 15, 429 (1975).

14. S. E. Buttrill, A. D. Williamson, and P. LeBreton, J. Chem. Phys., 62, 1586 (1975).

15. R. E. Huffman, Y. Tanaka, and J. C. Larrabee, Appl. Optics, 2, 617 (1963).

16. J. A. R. Samson, Techniques of Vacuum Ultraviolet Spectroscopy, (Wiley, N.Y., 1967).

17. K. E. Schubert and R. D. Hudson, Aerospace Corp. Report No. ATN-64(9233)-2, (Aerospace Corp., El Segundo, Ca., 1963).

18. R. E. Huffman, J. C. Larrabee, and D. Chambers, Appl. Optics, 4, 1145 (1965).

19. K. Watenabe, F. M. Matsunaga, and H. Sakai, Appl. Optics, 6, 391 (1967).

20. J. C. Person and P. P. Nicole, J. Chem. Phys., 53, 1767 (1970). A tabular presentation of the data is given in Argonne National Labs Radiological Division Annual Report, F41970, ANL-7760 Part I, pp. 97 - 109.

21. G. L. Weissler, J. A. R. Samson, M. Ogawa, and G. R. Cook, J. Opt. Soc. Am., 49, 338 (1958).

22. C. Lifshitz and W. A. Chupka, J. Chem. Phys., 47, 3439 (1967).

CHAPTER II

Ion-Molecule Reactions in Vinyl Fluoride by Photoionization. Effects of Vibrational Excitation on Major Reaction Pathways

I. Introduction

At pressures low enough to avoid collisional stabilization of the excited intermediate, the molecular ion in vinyl fluoride undergoes Reactions (1)-(3). The enthalpy of Reaction (1) is calculated

$$C_2H_3F^+ + C_2H_3F \longrightarrow [C_4H_6F_2^+]^* \begin{cases} \longrightarrow C_3H_5^+ + CHF_2\cdot & (1) \\ \longrightarrow C_3H_4F^+ + CH_2F\cdot & (2) \\ \longrightarrow C_3H_3F_2^+ + CH_3\cdot & (3) \end{cases}$$

to be -9 kcal/mole; the thermochemistry of Reactions (2) and (3) is not as well characterized, but they have been estimated to be exothermic by 12 and 16 kcal/mole, respectively.[1]

In recent years several groups have studied Reactions (1)-(3) using electron impact ionization, with differing conclusions concerning the kinetics and mechanism of these reactions.[2-5] These studies indicate that the overall reaction rate and product distribution are affected by changing the ionizing electron energy and thus the internal energy distribution of the reactant ion.[2, 4] Beyond this general agreement, different mechanistic conclusions seem to be supported by different experimental techniques. Using a medium-pressure single source mass spectrometer, Herman and Harrison[2] and McAskill and Harrison[3] observe clear indications of mixed second-order and third-order kinetics, each mechanism showing a characteristic product distribution. The ion cyclotron resonance (ICR) studies of O'Malley and Jennings[4] and Anicich and Bowers[5] show only second order kinetics, with a product distribution nearly identical to the third-order distribution of the single

source studies. More recently Sieck et al.[6] have studied Reactions (1)-(3) using photoionization by rare gas resonance lamps. Their data indicate that ions formed within .27 eV of threshold react with a product distribution similar to the ICR and single source third-order values, while ions formed 1.3 eV above threshold show initial product distributions and decay kinetics similar to those of the medium pressure instruments. Their results show that vibrational excitation alone is sufficient to cause the effects on the reaction kinetics.

The mixed kinetics of the single source data have been interpreted in terms of bimolecular steps using the assumption that the overall rate and product distribution for Reactions (1)-(3) are strongly affected by excess energy in the reactant ions.[2, 3, 5] The competition between reaction and deactivation of ions in different energy states then leads to mixed kinetics and a product ratio that varies with the extent of reaction. The data of McAskill and Harrison[3] could be fit with a model that assumed the distribution of initial states could be replaced by one composite excited state with a single effective rate of reaction and an effective deactivation rate. However, the ICR experiments could not be fit by this model without the assumption that all reactant ions were formed without excess excitation.

In view of the past interest in the vinyl fluoride system, we have undertaken a study to further clarify the dynamics of these reactions. Using the techniques of photoionization mass

spectrometry, we have made quantitative measurements of the dependence of Reactions (1)-(3) on the vibrational state of the reactant ion. The present work is an extension of our earlier study of ion-molecule reactions in ethylene[7] and uses the techniques of that study. The use of photoionization mass spectrometry for investigating ion-molecule reactions has been recently reviewed by Chupka.[8]

II. Experimental

The photoionization mass spectrometer used in this study has been described elsewhere.[7] The instrument has been modified slightly to facilitate data collection. The mass selected ions are presently detected by a Bendix Model 4501 Channeltron electron multiplier operated in a pulse-counting mode. The light detecting system was replaced by a scintillator-photomultiplier combination. A glass plate coated with sodium salicylate was placed in the back of the sample chamber. Fluorescence from the salicylate phosphor is detected by a small photomultiplier (RCA Model 8571) mounted inside the vacuum chamber. The photomultiplier current is measured by a Cary 401 vibrating reed electrometer, whose output is filtered and fed to a voltage to frequency converter. Digitized ion and photon signals are then counted by a Hewlett-Packard 5243 counter operated in ratio mode; this method yields a direct output proportional to the photoionization efficiency of the ion under study and assures that counting statistics remain independent of the ionizing light intensity. In order to correct for variations in the

quantum efficiency of the sodium salycilate phosphor, photoionization efficiency measurements on nitric oxide were made over the energy range of the present study. These data were compared with the absolute photoionization cross section data of Watenabe et al.[9] to obtain a measurement of the relative quantum efficiency of our phosphor over the wavelength range 1200-1100 Å and in turn to correct the photoionization efficiency data for vinyl fluoride and its ionic products.

Other modifications include addition of a servo system to control the wavelength drive of the monochromator and a small programmable controller for data collection. The monochromator servo system uses a stepping motor and an optical encoder mounted on the grating drive train of the monochromator to sense and adjust the position of the grating to a wavelength accuracy of 0.1 Å. The programmable controller supervises the data collection and allows up to 10 masses to be sequentially monitored by the mass spectrometer.

Corrections for the mass discrimination of our quadrupole mass filter were made by comparing 50 eV electron impact mass spectra of n-hexane taken on our instrument with those taken by ion cyclotron resonance, which has a known mass discrimination.

In the present studies the hydrogen line spectrum was the source of ionizing light. Monochromator slits were set at 100 μ, giving an optical resolution of about 1 Å FWHM. All measurements were taken at a nominal average ion exit energy of less

than .12 volt to minimize translational energy effects on the ion molecule reactions studied.

The ion cyclotron resonance spectrometer used in this study has been previously described.[10] Ion trapping studies were performed by the method of McMahon and Beauchamp,[11] as previously described. All experiments on both instruments were conducted at ambient temperatures.

III. Results

A. Internal Energy States Populated Near Threshold

The parent ion photoionization efficiency of vinyl fluoride is presented in Fig. 1a. The ionization cross section shows an abrupt onset at 10.363 ± .015 eV photon energy and a series of steps in the photon energy range 10.4 - 11.2 eV. The vibrational states of the molecular ion that correspond to these steps may be assigned using the photoelectron spectrum of vinyl fluoride shown in Fig. 1b. Fig. 1b, taken from a recent publication of Reinke et al.,[12] is in good agreement with an earlier spectrum published by Lake and Thompson.[13] According to the analysis of both groups, the major vibration excited on ionization is the C=C stretch, denoted as ν_1. The other two vibrational modes shown in Fig. 1b are assigned to a C-F stretch ν_2 and an in-plane C-F band stretch ν_3. Reinke et al.[12] give frequencies of 1570, 1300, and 500 cm^{-1}, respectively, for ν_1, ν_2 and ν_3. The small steps due to combinations involving ν_3 can be seen in the photoionization data. However, the spacing of lines in the exciting spectrum is not sufficiently dense to allow

Figure 1. Comparison of (a) the molecular ion photoionization efficiency of vinyl fluoride with (b) the photoelectron spectrum, taken from Ref. 12. There is good agreement between the two experiments concerning the thresholds and relative population of the lower vibrational levels of the molecular ion. Step assignments used in Table II are labeled.

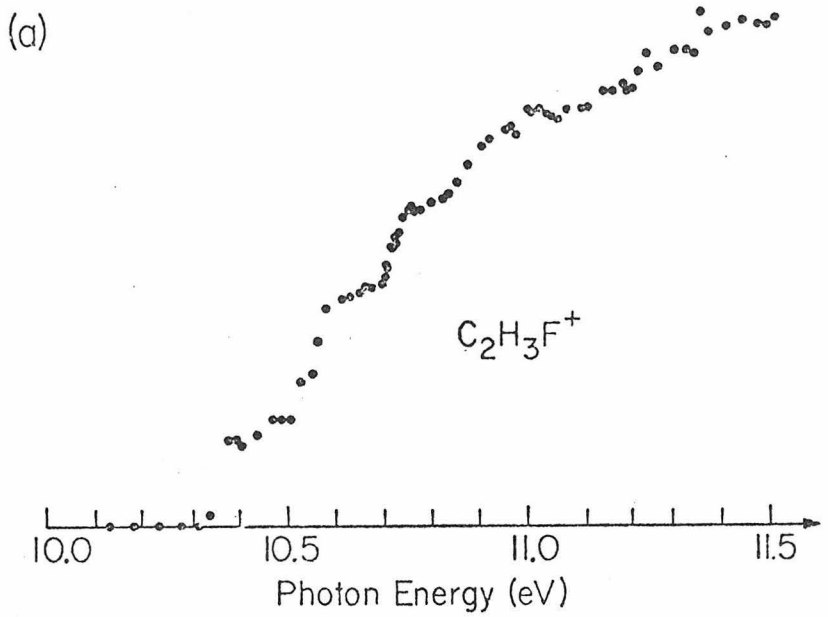
(a)
$C_2H_3F^+$
10.0
10.5
11.0
11.5
Photon Energy (eV)

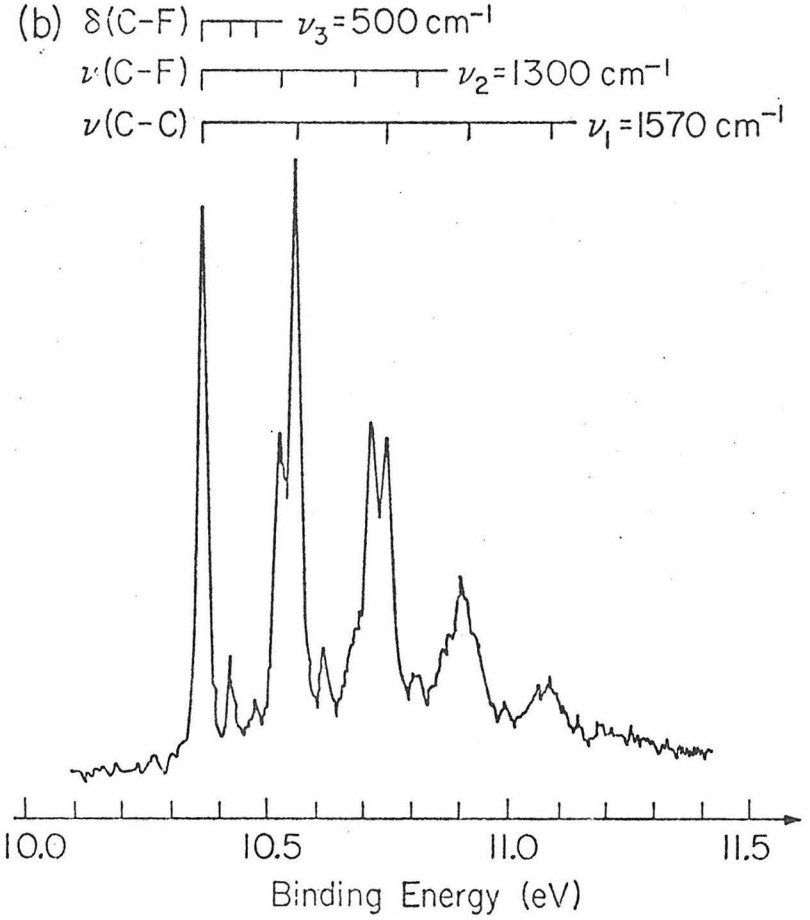
(b) δ(C-F) ν_3=500 cm^{-1}
ν(C-F) ν_2=1300 cm^{-1}
ν(C-C) ν_1=1570 cm^{-1}
10.0
10.5
11.0
11.5
Binding Energy (eV)

the states involving ν_1 and ν_2 to be distinguished. Thus, the steps chosen for use in this study and represented in Fig. 1a do not always represent a single vibrational state but rather a combination of two or more states with a narrow internal energy spread. The specific population of states comprising each step may be estimated by comparing Figs. 1a and 1b.

The photoionization mass spectrum of vinyl fluoride has also been studied by Reinke et al.[14] using synchrotron radiation as an ionization source. Their data agree well with the data of Fig. 1a in the photon energy range common to both studies. However, at photon energies from 11.2 to 13 eV they note a monotonic increase in the photoionization efficiency. Since the photoelectron spectrum shows no states accessible by direct ionization in this region, Reinke et al.[12, 14] attribute this structure to indirect ionization processes. Our raw data also show an increase in this photon energy region which can be attributed mostly to change in quantum efficiency of the sodium salycilate phosphor used in our study. When the data are corrected for the decrease in quantum efficiency of our scintillator, the rise with photon energy of our data becomes less dramatic. Our data indicate an increase in ionization efficiency of about 8% in the region from 11.5 eV to 12.0 eV which may be attributable to autoionization from a dense manifold of superexcited states in this region.

The lowest energy fragmentation process of the vinyl fluoride parent ion is loss of HF to form $C_2H_2^+$. We observe this

fragmentation at photon energies above 13.31 ± .05 eV. This is lower than the value of 13.51 ± .03 eV found by Reinke et al.,[14] a discrepancy which we are unable to explain. Our value is also 1.36 eV higher than the adiabatic appearance potential of 12.15 eV calculated from the heat of formation of $C_2H_2^+$ derived from acetylene. The fact that the measured appearance potential of $C_2H_2^+$ coincides with the second ionization potential of vinyl fluoride rather than the thermodynamic fragmentation threshold suggests that if autoionizing states are formed at photon energies above 12.15 eV, the ions produced do not retain sufficient internal energy to dissociate.

Our study of Reactions (1)-(3) is restricted to photon energies from 10.35 eV to 11.25 eV. It is assumed that the parent ions in this region are formed primarily by direct ionization and obey the step function threshold law. This assumption is justified by the excellent correspondence between the photoionization efficiency and photoelectron spectrum in this energy range, as well as the lack of obvious structure due to autoionization. Ions produced by autoionization will have an unknown distribution of internal energies and cannot be treated by the methods used in this study. Since the thresholds for several fragments coincide with the second ionization potential of vinyl fluoride, ions formed in electronically excited states are expected to decompose into fragments on a time scale rapid with respect to ion-molecule collision times and thus be unavailable for reaction. This

expectation is supported by the absence of a large increase in the parent ion photoionization efficiency above the threshold for the first electronically excited state of the ion. The expected increase in ionization cross section is restricted to fragment ions.[14] In view of these factors, our primary interest in this work is the Franck-Condon manifold of the ground electronic state of the vinyl fluoride parent ion.

B. Trapped Ion ICR Study of Vinyl Fluoride Reactions

Vinyl fluoride has not previously been studied using ICR trapped ion methods. Fig. 2 presents trapped ion data on the vinyl fluoride system at 11.5 eV electron energy, at which only the parent ion is formed. The qualitative features of the data are consistent with earlier studies.[2-6] The parent ion undergoes Reactions (1)-(3) with an overall disappearance rate constant measured as 2.9×10^{-10} cm^3 molecule^{-1} sec^{-1}. This number compares well with the value of 3.2×10^{-10} obtained by Sieck et al.[6] using 10.6 eV photons, and is in fair agreement with the values of 2.1×10^{-10} obtained by Anicich and Bowers[5] and 2.2×10^{-10} of McAskill and Harrison.[3]

As in previous studies, the products of Reactions (1) and (2) were found to react further by processes (4) and (5). In

$$C_3H_5^+ + C_2H_3F \longrightarrow C_5H_7F^+ + HF \qquad (4)$$

$$C_3H_4F^+ + C_2H_3F \longrightarrow C_5H_6F_2^+ + HF \qquad (5)$$

Figure 2. Variation of ion abundance with time in 2.8×10^{-6} torr of vinyl fluoride ionized at 11.5 eV. These data, obtained by ICR trapped ion techniques, yield a disappearance rate constant for $C_2H_3F^+$ of 2.9×10^{-10} cm^3 $molecule^{-1}$ sec^{-1}.

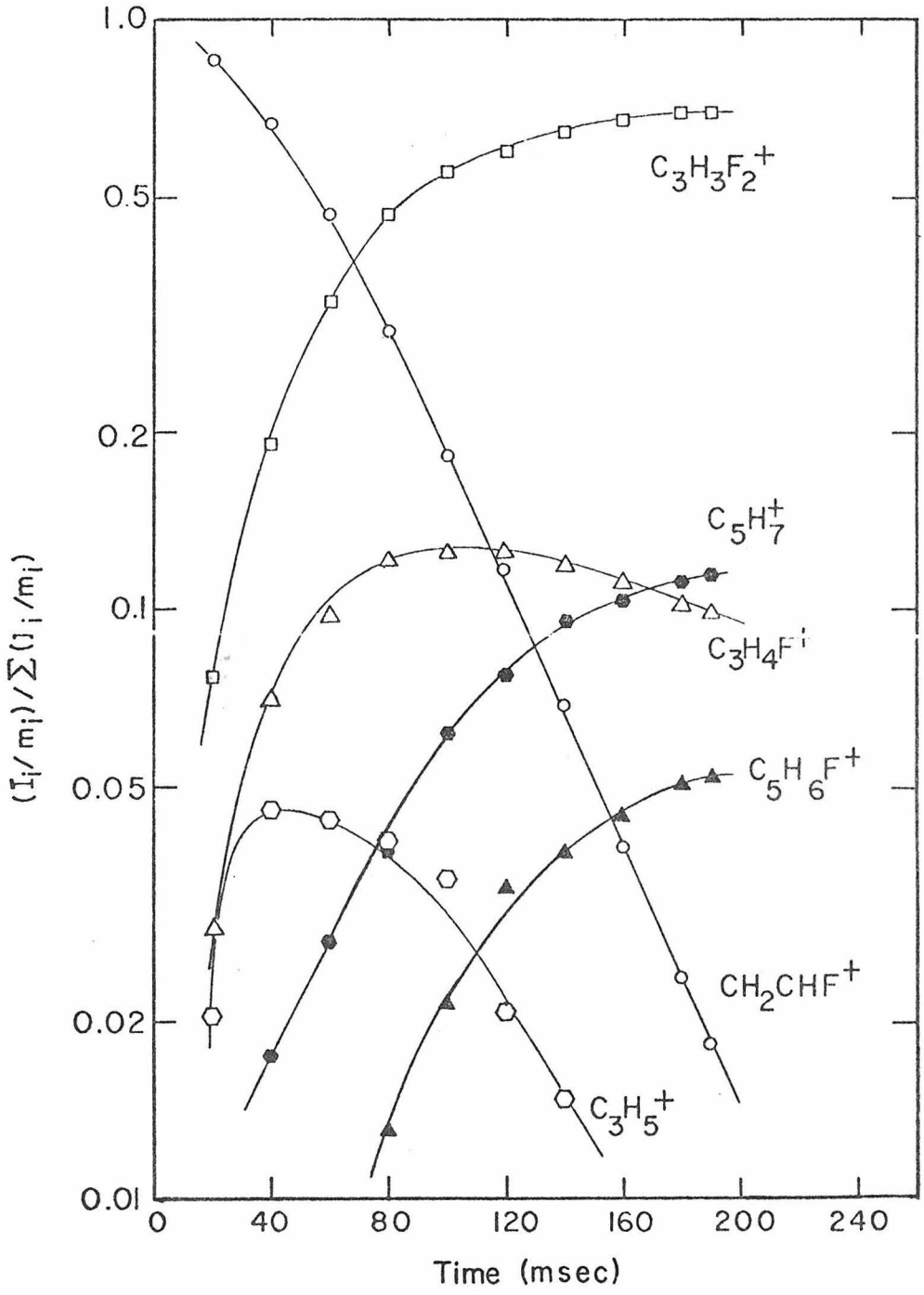
1.0
0.5
0.2
0.1
0.05
0.02
0.01
0
40
80
120
160
200
240
Time (msec)
$(I_i/m_i)/\Sigma(I_i/m_i)$
$C_3H_3F_2^+$
$C_5H_7^+$
$C_3H_4F^+$
$C_5H_6F^+$
CH_2CHF^+
$C_3H_5^+$

calculating product distributions, the product yields in Reactions (4) and (5) are added to those of their precursors.

The data in Fig. 2 are indicative of the participation of excited states in the reaction kinetics. There is a reproducible curvature in the parent ion decay. In addition, the relative product yields for Reactions (1)-(3) change in the course of the reaction from 0.20:0.24:0.56 at 15% conversion to 0.12:0.17:0.70 at 99% conversion.

C. Dependence of Reaction Cross Sections on Internal Energy

The photoionization efficiencies of the vinyl fluoride parent ion and two of the three secondary products are shown in Fig. 3. The third product ion, $C_3H_4F^+$, is omitted for clarity. These data, taken at less than 14% conversion to products, are normalized so that the three curves coincide at energies corresponding to the vibrational ground state of the parent ion. Given the assumption of step function threshold behavior, the heights of successive steps in the parent ion are proportional to the number of ions formed in the corresponding internal energy levels; the heights of successive steps in the product ions are proportional to the number of product ions formed by parent ions in the corresponding levels. For a particular state, the ratio of the product step height to the parent step height is proportional to the reaction cross section for parent ions in that state. Reaction cross sections obtained in this manner are summarized in Table I.

Figure 3. Photoionization efficiency data for vinyl fluoride reactant ion and product ions $C_3H_5^+$ and $C_3H_3F_2^+$. The third product ion, $C_3H_4F^+$, was omitted for clarity. Molecular ions in higher vibrational states exhibit decreased reactivity, particularly toward formation of the $C_3H_3F_2^+$ product

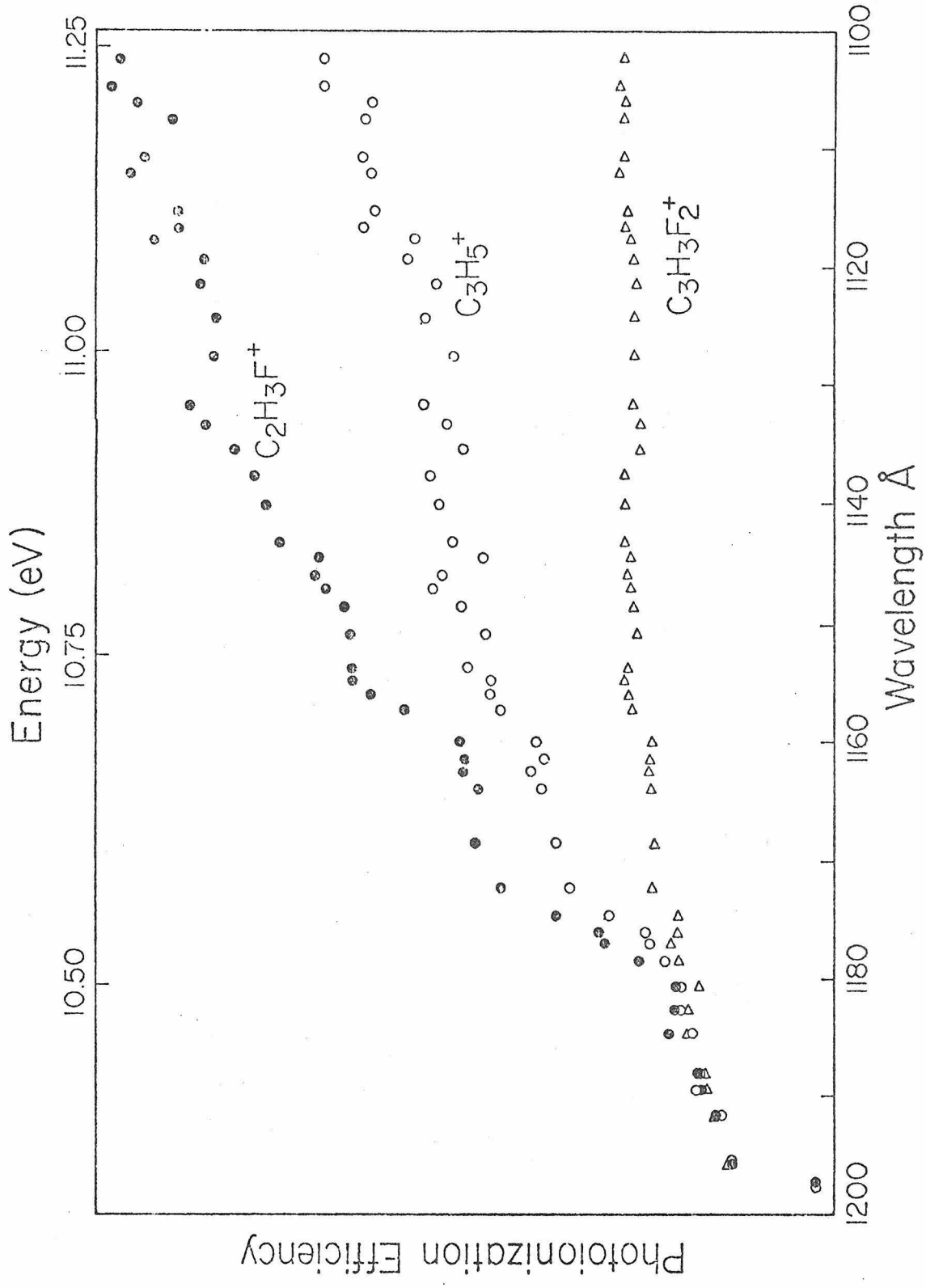
Photoionization Efficiency
Energy (eV)
11.25
11.00
10.75
10.50
Wavelength Å
1100
1120
1140
1160
1180
1200
$C_2H_3F^+$
$C_3H_5^+$
$C_3H_3F_2^+$

Table I. Relative Cross Sections for Reactions (1)-(3) for Lower Vibrational States of Vinyl Fluoride Reactant Ion

Step Number[a]	Major Vibrational States $\nu_1\nu_2\nu_3$[b]	Mean Internal Energy, eV	Relative Cross Sections[c] σ_1	σ_2	σ_3	σ_{Total}
1	000	0.00	0.086	0.121	0.792	1.000
2	001, 002	0.06	0.062	0.105	0.456	0.623
3	010, 100	0.18	0.060	0.100	0.159	0.319
4	101, 020, 110, 200	0.35	0.048	0.066	0.135	0.249
5	102, 030, 210, 300	0.53	0.037	0.039	0.052	0.128

[a]From Fig. 1a.

[b]Assignments from Ref. 12: ν_1 - C=C stretch; ν_2 - C-F stretch; ν_3 - in plane C-F bend. The list of states may not be exhaustive for each step.

[c]Normalized relative to the total cross section for ground state reactants.

The data in Fig. 3 and Table I allow some immediate conclusions. First, the cross sections for all three reaction channels decrease with increasing internal energy in the reactant ion. Second, the minor products show the least change with increasing internal energy, while the major Reaction (3) is dramatically affected. The addition of as little as .19 eV of vibrational energy to the parent ion reduces the probability of Reaction (3) by 80%. There is no evidence that the particular modes of vibration have distinguishable effects on the reaction cross section. The important factor appears to be only the mean vibrational energy content, consistent with the hypothesis of extensive randomization of internal energy in the activated intermediate.

In order to make a qualitative comparison with earlier data, total product distributions at photon energies corresponding to vibrational plateaus are listed in Table II along with earlier results under differing experimental conditions. Photons of 10.4 eV produce only ground state ions; higher energy photons form a distribution of vibrational states. As is expected from the data in Table II, increasing the number of ions in vibrationally excited states causes the fraction of the $C_3H_5^+$ and $C_3H_4F^+$ products to increase at the expense of the $C_3H_3F_2^+$ product. Some interesting comparisons may be made between product ratios from different published sources. For example, our product ratio at 10.65 eV agrees well with that of Sieck[6] at 10.6 eV and with the ICR results of Anicich and Bowers.[5] The "second order" distribution in the

Table II. Product Distribution at Different Ionization Conditions

Ionization Source	Product Distribution Reac. (1)	Reac. (2)	Reac. (3)	Apparent Total Reaction Rate[a]
A. Present Work				
10.40 eV photons	0.09	0.12	0.79	1.00
10.50 eV photons	0.09	0.13	0.78	0.91
10.65 eV photons	0.12	0.19	0.69	0.61
10.75 eV photons	0.13	0.20	0.67	0.53
10.85 eV photons	0.14	0.20	0.66	0.47
11.22 eV photons	0.16	0.21	0.63	0.41
B. Other Studies				
Sieck et al.[b]				
10.6 eV photons	0.10	0.19	0.71	3.2×10^{-10}
11.7 eV photons	0.26	0.27	0.46	
Anicich & Bowers[c]	0.09	0.18	0.72	2.1×10^{-10}
Herman & Harrison				
"Second Order"	0.27	0.33	0.40	1.3×10^{-11}[e]
"Third Order"	0.12	0.23	0.64	2.2×10^{-10}[e]
McAskill & Harrison				
"Second Order"	0.26	0.27	0.47	2.1×10^{-11}[e]
"Third Order"	0.15	0.21	0.65	2.3×10^{-10}[e]

[a]Represents reaction probability for low conversion. Present results are normalized to unity for 10.40 eV photons. Previous results are quoted rate constants in units of cm^3 $molecule^{-1}$ sec^{-1}. A rough correspondence may be obtained by multiplying present values by observed rate of 2.9×10^{-10} cm^3 $molecule^{-1}$ sec^{-1}.

Table II (Continued)

[b]Ref. 6.

[c]Ref. 5. Similar results given by Ref. 4.

[d]Ref. 2.

[e]Effective bimolecular reaction rate calculated in Ref. 5.

[f]Ref. 3.

works of Harrison's laboratory[2, 3] agrees with the 11.7 eV value of Sieck et al.[6] but indicates a higher degree of excitation than is seen in our work. Since direct ionization to states with ionization energies above 11.2 eV is not a favored process, the increase in the average excitation seen in these studies may be due to autoionization from superexcited neutral states in this energy region.

Previous studies indicate that collisional deactivation of excited vinyl fluoride ions is an efficient process.[2, 3, 5] In order to investigate the effects of collisional relaxation for ions in well characterized states, a study of the effect of pressure on Reactions (1)-(3) was performed. Variation of the fractional abundance of the $C_3H_3F_2^+$ product of Reaction (3) with vinyl fluoride pressure is shown in Fig. 4 for two photon energies. Ions formed at 10.41 eV photon energy are in the vibrational ground state. The 10.64 eV data correspond to the plateau of Step 3 in Fig. 1a. By comparing the photoionization and photoelectron data in Fig. 1, the population of specific vibrational states formed at 10.64 eV is found to be: 32% ground state, 12% $\nu_3 = 1$ or 2, 20% $\nu_2 = 1$, and 36% $\nu_1 = 1$. Thus, 68% of the ions are formed with a quantum of vibrational excitation, with a mean excitation energy of 1300 cm^{-1} or .16 eV. Since the cross section for Reaction (1) decreases by 75% for this distribution of excited ions, they may be distinguished from ground state ions by their reaction kinetics. The data were fit to the reaction scheme shown below. Using relative product distributions from Table I, k_1, k_2 and k_4 were calculated relative to k_3, which was fit using the 10.41 eV data, in which only ground state

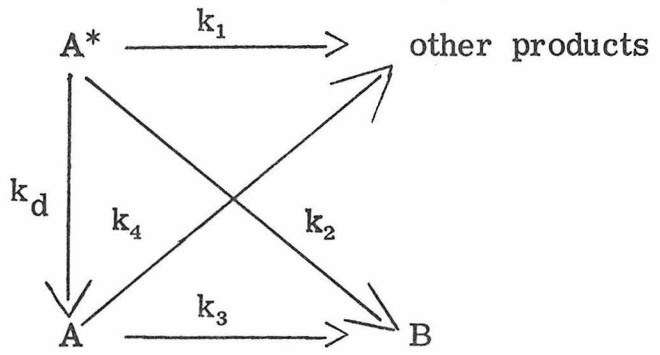

A = $C_2H_3F^+$

B = $C_3H_3F_2^+$

reactants are present. The 10.64 eV data were then fit by using the experimental distribution of initial states and adjusting k_d by a least squares method. As a result k_d was found to be (1.76 ± .15) times the value of k_3. Using $k_3 = 2.3 \times 10^{-10}$ cm^3 molecule^{-1} sec^{-1} from our ICR trapped ion data, we obtain k_d = $4.1 \pm 0.4 \times 10^{-10}$ cm^3 molecule^{-1} sec^{-1} for the distribution of ions formed in Steps 2 and 3 of Fig. 1a. Fits to the 10.64 eV data using the optimized k_d and $k_d = 0$ are shown in Fig. 4.

The only comparable calculations have been those of Anicich and Bowers[5] who used a model analogous to the one presented above (Mechanism Ia of Ref. 5) with the exception of their assumption that all ions are originally formed in the state A*. This model yields a deactivation rate of 3.5×10^{-10} cm^3 molecule^{-1} sec^{-1} for the data of McAskill and Harrison.[3] In view of the much higher degree of initial excitation in their system, it is somewhat surprising that their rate is in such good agreement with the value measured in the present work.

It is instructive to note that the 10.64 eV data could also be fit by a simple pseudo-first-order model with an effective rate of .52 times k_3, or 1.19×10^{-10} cm^3 molecule^{-1} sec^{-1}. This

Figure 4. Fractional abundance of $C_3H_3F_2^+$ product of Reaction (3) as a function of vinyl fluoride pressure for two photon energies corresponding to Steps (1) and (3) in the ionization efficiency of the parent ion shown in Fig. 1a. The lines represent fits to the data using the relative reaction efficiencies shown in Table I, as discussed in the text. Curves calculated for the 10.65 eV data are shown for (a) $k_d = 4.1 \times 10^{-10}$ cm^3 $molecule^{-1}$ sec^{-1} and (b) $k_d = 0$.

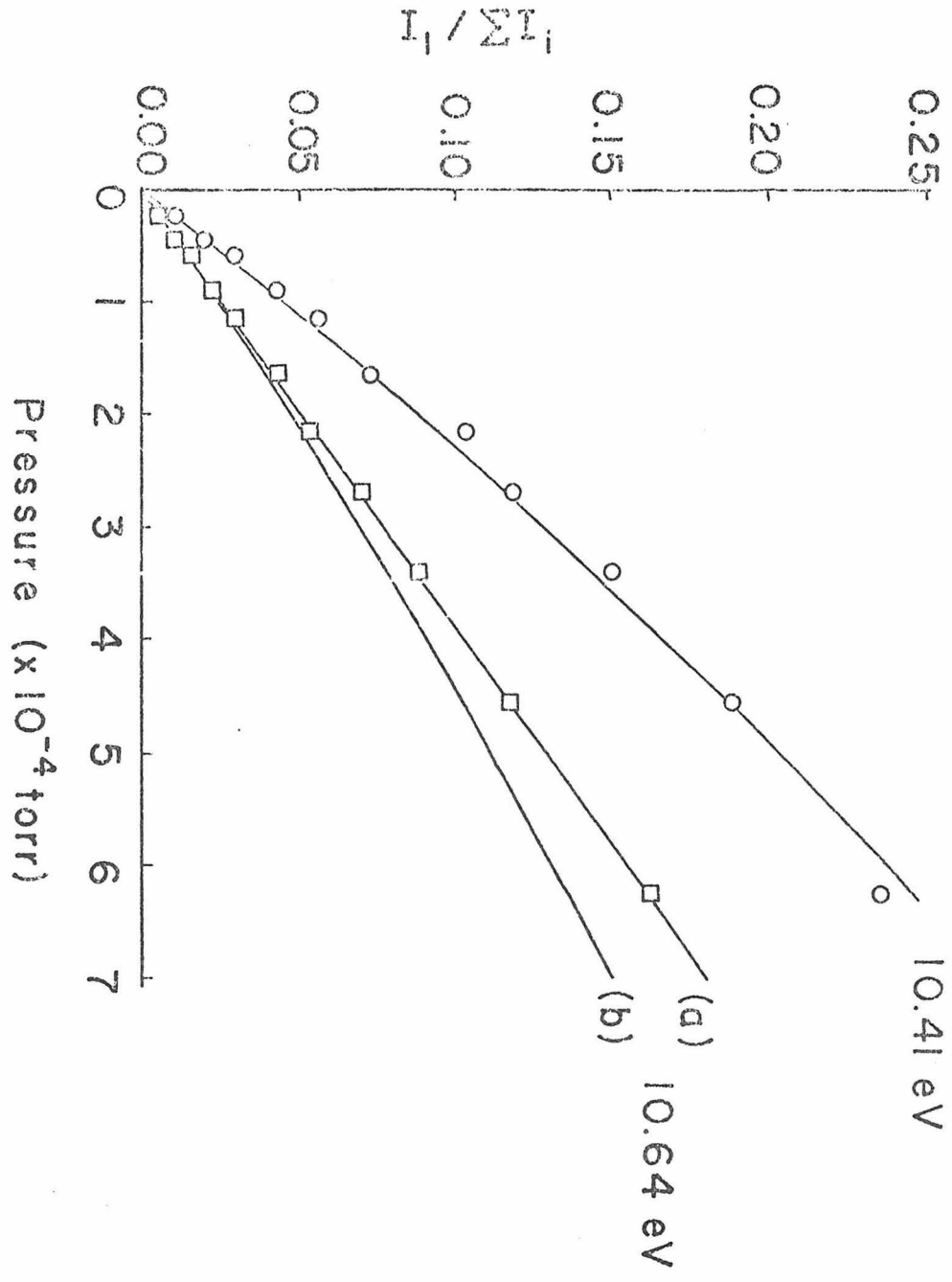
$I_i / \Sigma I_i$
0.00
0.05
0.10
0.15
0.20
0.25
0
1
2
3
4
5
6
7
Pressure (x 10^{-4} torr)
10.41 eV
(a)
10.64 eV
(b)

provides an excellent example that an approximately linear relationship between the fractional abundance of a product and pressure does not in itself guarantee a second order process.

IV. Discussion

The extreme sensitivity of Reactions (1)-(3) to internal excitation of the reactant ion explains much of the variation in the reported kinetics and product distribution of this system.[2-5] Past studies invariably populated a distribution of vibrational states of the parent ion. Thus, reaction rates measured at low conversion represent an average of the individual cross sections given in Table I weighted by the relative populations of the internal states. At higher conversions the population of states changes continually due to reaction and collisional deactivation. As a result the kinetics depart from pseudo-first order, and the product distribution changes with the extent of reaction. These effects are clearly seen in the data of Herman and Harrison,[2] McAskill and Harrison,[3] and Sieck et al.[6] The similarity in rate constants for relaxed ions determined by those workers with those of the present study is gratifying, as is the agreement in the deactivation rates calculated for our study and those calculated[5] for the data of McAskill and Harrison.[3]

It is not completely clear why the earlier ICR studies[4,5] could not be fit by the model of Anicich and Bowers[5] without the assumption that essentially all ions were in their ground state. Certainly, the ICR product distributions indicate a low degree of

excitation. However, we feel there are indications that excited states do participate in the ICR experiment. First, our ICR trapped ion data, with a longer time scale and higher conversion does show a changing reactivity with time. Secondly, O'Malley and Jennings[4] do report a change in product ratios with electron energy, indicating a changing vibrational population. Finally, we note that pure second order kinetics are not guaranteed by apparent linearity in the growth of product ions at low conversion, as mentioned previously in connection with Fig. 4.

Some differences may be noted between the vinyl fluoride system and the analogous reaction in ethylene.[7] Primarily, the available states of the molecular ion differ for the two systems. At 13 eV photon energy 70% of the ethylene molecular ions formed are initially in the $^2B_3$ first excited state. In vinyl fluoride the thermodynamic appearance potential for the lowest energy fragmentation lies below the first electronically excited state, and the parent ion efficiency curve does not exhibit the dramatic increase in this state seen in the ethylene system. This indicates that most if not all electronically excited vinyl fluoride ions decompose before reaction can occur. As a result, when moderate (> 15 eV) ionizing energies are used the effects of vibrational energy are expected to be more significant experimentally in vinyl fluoride, while the major effects noted in ethylene are due to ions formed in the first electronically excited state (where internal conversion to highly vibrationally excited ground state ions may precede reaction).

A second quantitative difference in the two systems is the greater sensitivity to internal excitation of the vinyl fluoride system, particularly Reaction (3). One factor that may be of importance here is the different reaction efficiencies for ground state ions in the two systems. Ion molecule reactions in ethylene occur on almost every collision, whereas in vinyl fluoride the reaction rate is only 19% of the collision rate.[15] One possible explanation assumes that in each system the initially formed intermediate must rearrange before any product channels are available. If the ratio of decomposition rate to rearrangement rate is higher in the vinyl fluoride case than in ethylene, the relative reaction efficiencies follow. Added internal energy would further increase the decomposition rate in both systems, but if the rearrangement is initially much faster than decomposition in ethylene (as appears to be the case) then the vinyl fluoride system would be more sensitive to this decrease in lifetime of the initially formed complex.

Some insight into the mechanism of Reactions (1)-(3) may be gleaned from recent work. In a comprehensive study of reactions in mixtures of different fluoroethylenes, Anicich and Bowers[15] present convincing evidence that the reactions in these systems involve cyclobutane intermediates that may open to a tetramethylene structure, rearrange by H or F atom migration, and eliminate a $C(H, F)_3$ radical to form products. One such system in their study is Reactions (6)-(9) in a mixture of ethylene and cis- or trans- 1, 2 difluoroethylene. This system produces both the reactants and

$$CH_2CH_2^+ + \underline{cis}\text{-}CHFCHF \longrightarrow \begin{cases} \xrightarrow{28\%} C_2H_3F^+ + C_2H_3F & (6) \\ \xrightarrow{11\%} C_3H_5^+ + CHF_2\cdot & (7) \\ \xrightarrow{20\%} C_3H_4F^+ + CH_2F\cdot & (8) \\ \xrightarrow{41\%} C_3H_3F_2^+ + CH_3\cdot & (9) \end{cases}$$

products of Reactions (1)-(3) in vinyl fluoride, suggesting that the cyclobutane intermediate I may be common to both systems. In the vinyl fluoride system intermediate II is also possible. Anicich

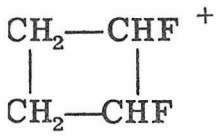

I

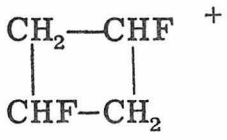

II

and Bower[15] report studies of Reactions (6)-(9) with ethylene-d_4 as a reactant. The C_3 products contained all possible isotopic compositions, including two ($C_3H_2D_3^+$ and $C_3D_3F_2^+$) which could not arise from a single atom migration. However, no isotopic scrambling occurs in the vinyl fluoride product of Reaction (6). These findings indicate that the decomposition of intermediate I, while complex, is still more specific than a total scrambling model would indicate.

While our data do not implicate specific intermediates or mechanisms for Reactions (1)-(3), several related studies may be proposed which would yield a more definitive understanding of this system. In our earlier study of ethylene[7] it proved illuminating to

compare the effects of internal energy on the decomposition modes of the $[C_4H_8^+]^*$ intermediate with the distribution of products observed for the decomposition of cyclobutane molecular ions formed with reasonably well characterized internal energy. Likewise it would be helpful to conduct a charge exchange or photoionization mass spectrometric study of the fragment distribution of the 1, 2- and 1, 3-difluorocyclobutanes as a function of internal energy. These data could be related to the product distributions of intermediates I and II, respectively, as functions of internal energy. An independent study of intermediate I formed by an ion-molecule reaction pathway involves study of Reactions (6)-(9) by the methods used in the present work, varying internal energy in either ethylene or difluoroethylene as the ionic reactant. Use of isotopically labeled reactants may yield information on the barrier to specific H or F atom migrations.

References

1. From Ref. 5 and sources listed therein. The value of $\Delta H_f^{298}(C_3H_5^+)$ is assumed to be 224 ± 2 kcal/mole, from S. E. Buttrill, A. D. Williamson, and P. LeBreton, J. Chem. Phys. 62, 1586 (1975).
2. J. A. Herman and A. C. Harrison, Can. J. Chem. 47, 957 (1969).
3. N. A. McAskill and A. C. Harrison, Int. J. Mass Spectrom. Ion Phys. 5, 193 (1970).
4. R. M. O'Malley and K. R. Jennings, Int. J. Mass Spectrom. Ion Phys. 2, 441 (1969).
5. V. G. Anicich and M. T. Bowers, Int. J. Mass Spectrom. Ion Phys. 12, 231 (1973).
6. L. W. Sieck, R. Gorden, S. G. Lias and P. Ausloos, Int. J. Mass Spectrom. Ion Phys. 15, 181 (1974).
7. P. R. LeBreton, A. D. Williamson, J. L. Beauchamp, and W. T. Huntress, J. Chem. Phys. 62, 1623 (1975).
8. W. A. Chupka, "Ion-Molecule Reactions by Photoionization Techniques," in Ion Molecule Reactions, J. L. Franklin, ed. (Plenum, N.Y., 1972).
9. K. Watenabe, F. M. Matsunaga, and H. Sakai, Appl. Opt. 6, 391 (1967).
10. M. S. Foster and J. L. Beauchamp, J. Amer. Chem. Soc., in press.

11. T. B. McMahon and J. L. Beauchamp, Rev. Sci. Instr. 43, 509 (1972).

12. D. Reinke, H. Baumgärtel, T. Cvitaš, L. Klasinc, and H. Güsten, Ber. Bunsen-Gesellschaft 78, 1145 (1974).

13. R. F. Lake and H. Thompson, Proc. Roy. Soc. Lond. A315, 323 (1970).

14. D. Reinke, R. Kraessig, and H. Baumgärtel, Z. Naturforsch. 28A, 1021 (1973).

15. V. C. Anicich and M. T. Bowers, Int. J. Mass Spectrom. Ion Phys. 13, 359 (1974).

CHAPTER III

Effects of Vibrational Energy on the Reactivity of Ketene Molecular Ions by Photoionization Mass Spectrometry

1. Introduction

Ion-molecule reactions in ketene have been the subject of recent ion cyclotron resonance (ICR) studies in our laboratories [1]. In this work we report detailed studies by photoionization mass spectrometry of the reactions of the molecular ion in ketene and ketene-d_2, particularly the dependence of reaction cross sections on vibrational state of the reactant ion.

This work also provides a spectroscopic limit to the heat of formation of neutral ketene. There are two prior studies of this quantity in the recent literature. Calorimetric measurements by Rice and Greenberg [2] in 1934 yielded a value of $\Delta H_f^{298}(CH_2CO) = -14.78$ kcal/mole. Nuttall et al. [3] recently noted that this value led to a predicted threshold of 3580 Å for the photolysis of ketene to yield CH_2 and CO. Since they had observed photolysis at wavelengths up to 3690 Å, they repeated the calorimetric work of Rice and Greenberg, obtaining $\Delta H_f^{298}(CH_2CO) = -11.4 \pm 0.4$ kcal/mole. The photolytic study of Nuttall et al. [3] exemplifies the use of spectroscopic measurements, in this case fragmentation thresholds, to infer thermochemical data relating a parent molecule and its fragments. Other workers, such as Setser [4] and Okabe [5], have exploited this technique extensively. Our work utilizes a complementary methodology by relating the ketene molecule and its reaction products through measurement of an energy threshold for the endothermic process (1).

$$CH_2CO^+ + CH_2CO \rightarrow C_2H_4^+ + 2CO \qquad (1)$$

The energy resolution and threshold laws of photoionization allow the formation of reactant ions with well characterized internal energy distributions [6].

2. Experimental

The ICR studies were performed on an instrument built in the Caltech shops, which has been previously described [7]. The photoionization instrument and its operation have also been described in detail [8]. The present studies utilized the molecular hydrogen line spectrum at 1 Å bandpass as a photoionization source. To avoid effects due to translational excitation, low repeller voltages were used to extract ions from the reaction chamber. Nominal ion exit energies were ~0.1 eV. Ketene pressures of 1.4×10^{-4} torr were used, giving approximately 15% conversion of ketene molecular ion to products.

Ketene was synthesized by low pressure pyrolysis of acetic anhydride at 500°C [9], and purified by passage through a dry ice-acetone cooled trap which collected involatile byproducts and unreacted anhydride. Ketene was collected in a second trap at liquid nitrogen temperatures and was further purified by additional bulb-to-bulb distillations at low temperatures. Ketene-d_2 was prepared in the same manner using acetic anhydride-d_6.

3. Results and Discussion

Figure 1 shows ICR trapped ion data on the variation of ion

Fig. 1. Variation of ion abundance with time in 1.3×10^{-6} torr of ketene ionized by a 10 msec electron beam pulse.

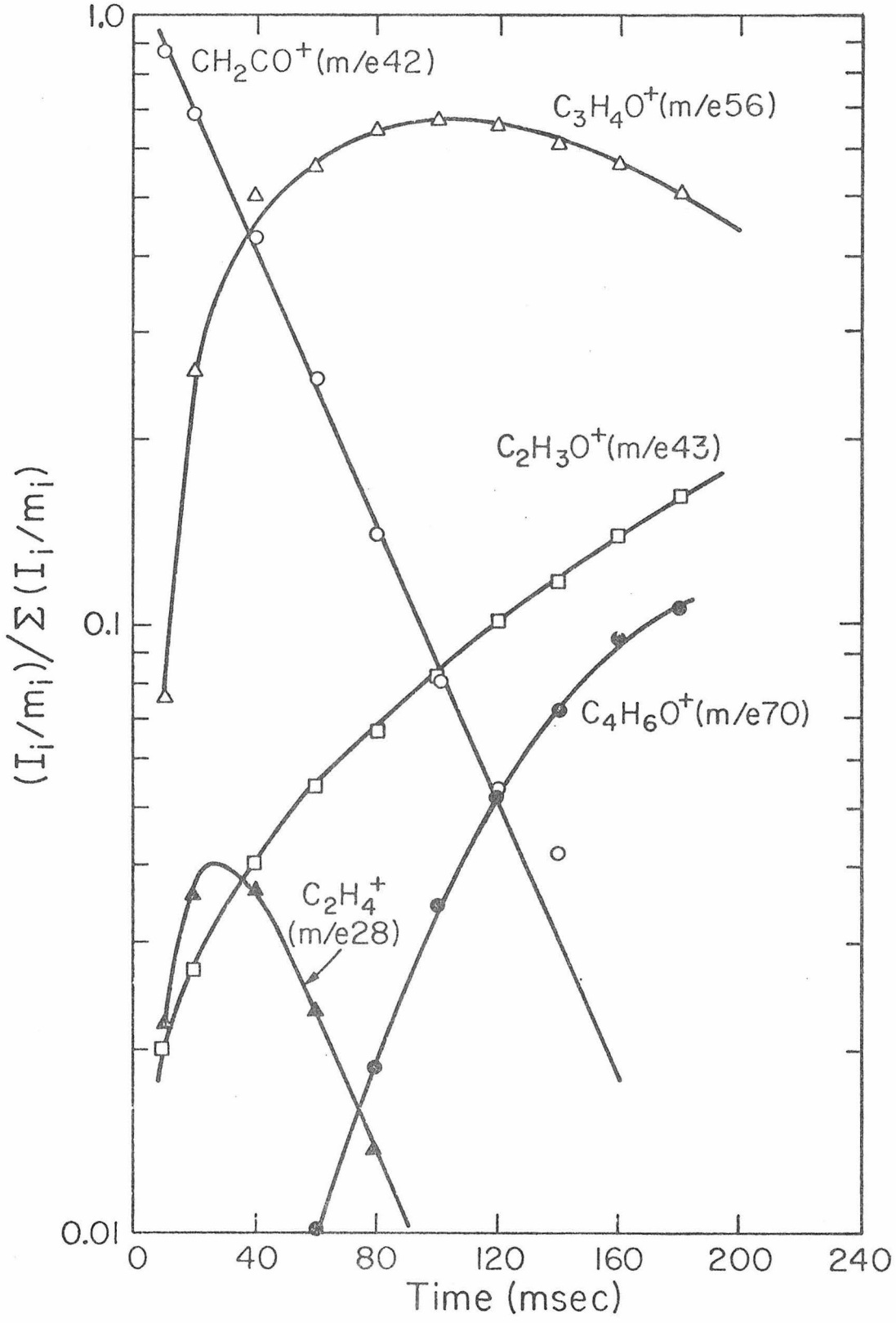
1.0
0.1
0.01
$(I_i/m_i)/\Sigma(I_i/m_i)$
CH_2CO^+(m/e42)
$C_3H_4O^+$(m/e56)
$C_2H_3O^+$(m/e43)
$C_4H_6O^+$(m/e70)
$C_2H_4^+$
(m/e28)
0
40
80
120
160
200
240
Time (msec)

abundance with time in ketene ionized under conditions such that only the molecular ion is initially present. Use of ketene-d_2 and double resonance techniques allow positive identification of the reaction pathways involved.

The processes involving ketene molecular ions are reactions (1)-(3). The ICR data of fig. 1 yield an overall rate of 5.9×10^{-10} cm^3

$$CH_2CO^+ + CH_2CO \rightarrow [C_4H_4O_2^+]^* \begin{cases} \rightarrow C_2H_4^+ + 2CO & (1) \\ \rightarrow C_3H_4O^+ + CO & (2) \\ \rightarrow C_2H_3O^+ + C_2HO & (3) \end{cases}$$

$molecule^{-1}sec^{-1}$ for disappearance of ketene molecular ions through these three channels. The major reaction pathway is process (2), involving loss of CO. The $C_3H_4O^+$ product then undergoes reactions (4) and (5), involving, respectively, proton transfer to neutral ketene,

$$C_3H_4O^+ + CH_2CO \begin{cases} \xrightarrow{78\%} C_2H_3O^+ + C_3H_3O & (4) \\ \xrightarrow{22\%} C_4H_6O^+ + CO & (5) \end{cases}$$

and abstraction of the CH_2 from the reactant neutral. The ionic product of process (5) in turn reacts with ketene, adding another methylene to form $C_5H_8O^+$. Reaction (4) is the source of most of the $C_2H_3O^+$ ion observed in fig. 1; proton transfer from the ketene molecular ion (reaction 3) accounts for only 11% of the reaction products derived from the parent ion. The ethylene molecular ion produced in process (1) reacts by charge transfer to regenerate

the ketene molecular ion, leading to the overall sequence shown in table 1. As noted in table 1, the overall sequence is exothermic and would lead to the decomposition of ketene in a chain reaction. The first step, reaction (1), is calculated to be endothermic for ground state reactants. The data of Nuttall et al. [3], predict the enthalpy of reaction (2) to be 3.1 kcal/mole; the older data of Rice and Greenberg [2] give 10.1 kcal/mole for the same quantity. The enthalpy change for reaction (1) involving ketene-d_2 can be calculated. Since photoionization measurements indicate no significant isotope effect on the ionization potential of ketene or ethylene [10], the thermodynamic isotope effect on ion-molecule reaction (1) is identical to that of its neutral analog. This quantity was estimated using the vibrational frequencies of Moore and Pimentel [11] for ketene and ketene-d_2 and those of Arnett and Crawford [12] for ethylene and ethylene-d_4. As a result, the enthalpy of reaction (1) was found to be only 0.14 kcal/mole less for ketene-d_2 than for ketene itself.

The preceding data suggest a sensitive test to distinguish the two reported values for the heat of formation of ketene. Theories of ion-molecule reaction dynamics [13] predict that increased internal energy in the reactants will lead to a decrease in the cross section for exothermic reaction channels. At 0°K the cross sections of endothermic channels will show an onset at an energy equal to the reaction endothermicity and will increase with internal

Table 1

Thermochemistry of reaction (1)

Reaction	ΔH^a(kcal/mole)	
	NLK[b]	RG[c]
$CH_2CO^+ + CH_2CO \rightarrow C_2H_4^+ + 2CO$	3.3	10.1
$C_2H_4^+ + CH_2CO \rightarrow CH_2CO^+ + C_2H_4$	-20.8	-20.8
Overall Process $2CH_2CO \rightarrow C_2H_4 + 2CO$	-17.5	-10.7

a) Using data from Ref. [16].

b) Using $\Delta H_f^{298}(CH_2CO) = -11.4$ kcal/mole, Ref. [3].

c) Using $\Delta H_f^{298}(CH_2CO) = -14.8$ kcal/mole, Ref. [2].

energy. At 298°K the thermal energy of the reactants will result in a non-zero cross section below the 0°K threshold, but the qualitative behavior of the cross section will not be altered. These expectations have been experimentally verified for reactions of rare gas atoms with hydrogen molecular ions [13, 14]. Thus the cross section of reaction (1) as a function of the internal energy of the reactant should exhibit a sharp increase in the vicinity of threshold. The threshold thus determined may be used to calculate the heat of formation of ketene.

The photoelectron spectrum of ketene reveals the internal energy states of the parent ion which are accessible by direct photoionization. Spectra taken in our laboratory show a vibrational band with a spacing of 2240 ± 80 cm^{-1} for both isotopic species, and a second band of the same frequency offset by 1090 ± 80 cm^{-1}. Since neither vibration exhibits an isotopic shift, Turner's [15] assignments of the major vibration as the C–O stretch ν_2 and the minor vibration as the C–C stretch ν_4 seem reasonable. Our spectra differ from Turner's only in that his value of 9.64 eV for ketene [15] does not agree with our value of 9.61 ± 0.01 eV by photoelectron spectroscopy or 9.614 ± 0.008 eV for both isotopic species by photoionization mass spectrometry.

The photoionization efficiency of the parent ion in ketene-d_2 is shown as circles in fig. 2. The states found in the photoelectron spectrum occur as a distinct steps in fig. 2, suggesting that direct ionization rather than autoionization predominates in this system.

Fig. 2. Photoionization efficiency of molecular ion and product ions of reactions (1) and (2) in ketene-d_2. Arrows indicate thresholds calculated for reaction (2) using (a) data of Nuttall et al. [3]; (b) data of Rice and Greenberg [2].

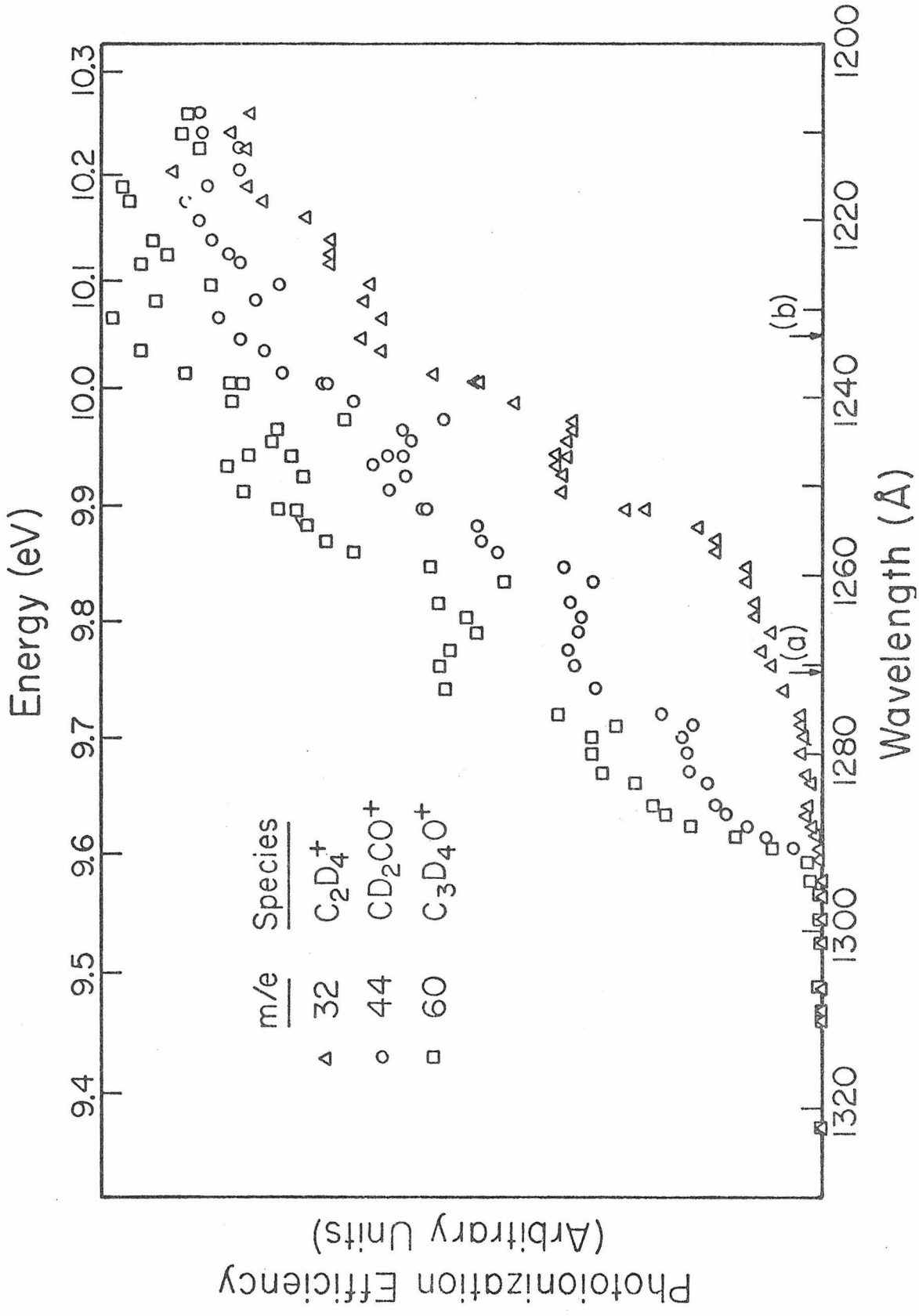
Photoionization Efficiency
(Arbitrary Units)
Energy (eV)
9.4
9.5
9.6
9.7
9.8
9.9
10.0
10.1
10.2
10.3
Wavelength (Å)
1320
1300
1280
1260
1240
1220
1200
m/e
Species
32
$C_2D_4^+$
44
CD_2CO^+
60
$C_3D_4O^+$
(a)
(b)

Also shown in fig. 2 are the products of reactions (1) and (2). In the deuterated compound the product of reaction (1) has m/e 32, confirming its molecular composition as $C_2D_4^+$. No m/e 28 ion was observed, giving confidence to our assumption that the ion of this mass in normal ketene is exclusively $C_2H_4^+$. This result is to be expected, since the threshold for forming CO^+ as a reaction product is expected to be 3.50 eV higher than that of reaction (1) with CO and ethylene as the neutral products and 3.11 eV higher with acrolein the neutral product [16].

The vertical arrows in fig. 3 correspond to calculated thresholds for reaction 1 using the differing values of the heat of formation of ketene.

Using the assumption that the height of each step in the photoionization efficiency curve is proportional to the number of ions formed in the corresponding vibrational level, relative cross sections for reactions (1-3) have been calculated for both isotopic species and are summarized in table 2. As is evident from fig. 2 and table 2, the cross section for reaction (1) is small for ground state ketene ions and increases by an order of magnitude as vibrational energy is added to the reactant ion. In contrast the cross section for reaction (2) decreases slightly, as is often observed for an exothermic reaction which is rapid at thermal energies. The data in fig. 2 and table 2 are clearly consistent with the data of Nuttall et al. [3], and do not support the earlier study.

Table 2

Cross sections for reactions (1)-(3) for lower vibrational levels of reactant ion.[a]

Vibrational State		Reactions in CD_2CO				Reactions in CH_2CO[b]		
ν_2	ν_4	σ_1	σ_2	σ_3	σ_{total}	σ_1	σ_2	σ_{total}
0	0	0.04	1.00	0.04	1.08	0.02	1.00	1.02
0	1	0.24	0.71	0.03	0.98	0.09	0.68	0.77
1	0	0.65	0.67	0.06	1.28	0.22	0.72	0.94
1	1	0.82	0.50	0.07	1.39	0.59	0.37	0.96

a) Cross sections are normalized relative to σ_2 for ground state reactant ions.

b) Cross section for reaction (3) was not calculated due to interference from ^{13}C isotope peak of parent ion at the same mass.

The ion-neutral collision rate in ketene computed by the theory of Gioumousis and Stevenson [17] is 1.0×10^{-9} $cm^3 molecule^{-1}$ sec^{-1}, which is a lower limit to the true collision rate due to the permanent dipole moment of ketene [18]. Comparison with the total rate measured in our ICR study shows that reaction does not occur in at least 40% of the molecular ion-neutral encounters. The data in table 2 indicate that the total cross section for reactions (1)-(3) remains approximately constant over the internal energy range studied. The probability of unreactive collisions is essentially unaffected in comparison to changes in the product distribution. This constancy of the total reaction probability suggests that the observed variation of cross sections with vibrational energy is due to competition among the various reaction channels. Furthermore, unless there exists some concerted route to eliminate two CO species simultaneously from the intermediate complex, CO elimination must occur in a stepwise manner; that is, the products of reaction (1) must in turn arise from decomposition of $C_3H_4O^+$ formed by reaction (2).

The findings summarized above suggest a possible mechanism for reactions (1) and (2). According to this view, the two major reactions proceed through a common intermediate, which decomposes by loss of a single CO molecule. As internal energy in excess of the threshold of reaction (1) is added to the intermediate, the probability increases that sufficient excess energy will be partitioned to

the $C_3H_4O^+$ initial product to exceed its threshold for dissociation to $C_2H_4^+ + CO$.

This mechanism offers a possible explanation for the difference in the threshold behavior of reaction (1) when isotopically substituted reactants are used. At a given internal energy, the $C_3D_4O^+$ product of the first CO loss in ketene-d_2 has a higher density of vibrational states than does $C_3H_4O^+$ in ketene due to the lower vibrational frequencies of the deuterated ion. Thus it is expected that during the initial CO loss, relatively less of the energy of the reaction intermediate will be partitioned into internal modes of $C_3H_4O^+$ than will be the case for the deuterated species. Since less of the original energy of the reactants is then available for decomposition of $C_3H_4O^+$, the cross section for this channel (reaction 1) is expected to rise more slowly with reactant internal energy in ketene than in ketene-d_2.

References

[1] J. Vogt, A. D. Williamson and J. L. Beauchamp, to be published.

[2] F. O. Rice and J. Greenberg, J. Amer. Chem. Soc., 56 (1934) 2268.

[3] R. L. Nuttall, A. H. Laufer and M. V. Kilday, J. Chem. Thermodynamics, 3 (1971) 167.

[4] J. A. Coxen, D. W. Setser and W. H. Duewer, J. Chem. Phys. 58 (1973) 2244.

[5] H. Okabe and V. H. Dibeler, J. Chem. Phys. 59 (1973) 2430.

[6] W. A. Chupka, "Ion Molecule Reactions by Photoionization Techniques" in: Ion Molecule Reactions, ed. J. L. Franklin (Plenum, N.Y., 1972).

[7] M. S. Foster and J. L. Beauchamp, J. Amer. Chem. Soc., in press.

[8] P. R. LeBreton, A. D. Williamson, J. L. Beauchamp and W. T. Huntress, J. Chem. Phys. 62 (1975) 1623.

[9] A. D. Jenkins, J. Chem. Soc. 1952 (1952) 2563.

[10] R. Botter, V. H. Dibeler, J. A. Walker and H. M. Rosenstock, J. Chem. Phys. 45 (1966) 1198.

[11] C. B. Moore and G. Pimentel, J. Chem. Phys. 38 (1963) 2816.

[12] R. L. Arnett and B. L. Crawford, Jr., J. Chem. Phys. 18 (1950) 118.

[13] J. C. Light, J. Chem. Phys. 40, (1964) 3221; J. C. Light and J. Lin, J. Chem. Phys. 43 (1965) 3209.

[14] W. A. Chupka and M. E. Russell, J. Chem. Phys. 49 (1968) 5426.

[15] D. W. Turner, C. Baker, A. D. Baker and C. R. Brundle, Molecular Photoelectron Spectroscopy (Wiley-Interscience, London, 1970).

[16] J. L. Franklin, J. A. Dillard, H. M. Rosenstock, J. T. Herron, K. Draxl and F. H. Field, Natl. Std. Ref. Data Ser., Natl. Bur. Std., No. 26 (1969).

[17] G. Gioumousis and D. P. Stevenson, J. Chem. Phys. 29 (1958) 294.

[18] T. Su and M. T. Bowers, J. Chem. Phys. 58 (1973) 3027.

CHAPTER IV

Photoionization Mass Spectrometry of 2-Fluoropropane and 2,2-Difluoropropane. A Novel Determination of the Proton Affinity of Vinyl Fluoride and 1,1-Difluoroethylene.

Introduction

In past years systematic studies of photoionization efficiencies have been reported for parent and fragment ions derived from lower alkanes[1,2], ketones[3], and alcohols[4] but none of the alkyl fluorides have been studied except methyl fluoride[5]. In view of the ability of photoionization mass spectrometry to determine accurate appearance potentials for fragmentation processes, the lack of such studies has left a considerable gap in our knowledge of the thermochemical properties of organic molecules and ions containing fluorine.

There have been several recent studies of gas phase acid-base chemistry which provide insight into the thermochemistry of fluorocarbons. Fluoride transfer reactions have been shown to be fast and to provide knowledge of relative $R^+ - F^-$ heterolytic bond energies[6-8]. Proton affinity measurements on the fluoroethylenes have been performed by Ridge[9] which allow independent determinations of the heats of formation of the fluorinated ethyl cations. Likewise, limits on the enthalpy of formation of the $:CF_2$ radical have been determined using proton transfer reactions from CF_2H^+ [10]. Similar studies have been performed on the reactions of F^- and other conjugate bases with fluoroalkenes[11] and on the effects of fluorine substitution on gas phase acidities[12]. A factor that hinders our understanding of these systems is the difficulty of making accurate calorimetric measurements in fluorinated systems. Previous studies of fluoride-transfer reactions[6,7] have uncovered inconsistencies which can be resolved only if the heats of formation used for neutral species are considered to be in error.

In order to provide more precise heat of formation data on these systems and to fill in the gap of photoionization mass spectral data on fluoroalkanes, a series of photoionization studies on these systems has been undertaken in our laboratories. We wish to report here measurements on 2,2-difluoropropane and 2-fluoropropane. Heats of formation of neutral and ionic species in these systems are derived. In addition, a novel measurement of the proton affinities of vinyl fluoride and 1,1-difluoroethylene without reference to the heats of formation of the neutral species is presented.

Experimental Section

The photoionization mass spectrometer used for these studies has been described in detail[13,14]. For these studies the hydrogen molecular spectrum at 1 Å FWHM resolution was used as the source of ionizing radiation. Sample pressures were $\sim 8 \times 10^{-5}$ torr as measured by an MKS Baratron capacitance manometer. Repeller voltages of ~ 0.1 V were used, yielding an ion residence time of approximately 50 μsec. When appropriate, ion signals were corrected for ^{13}C isotope contributions. All experiments were performed at ambient temperature (20 - 25°C).

2-Fluoropropane was prepared in our laboratory from the reaction of AgF and isopropyl iodide[15] and purified by gas chromatography. The sample of 2,2-difluoropropane was purchased from Cationics, Inc.

Results

2,2-Difluoropropane

Photoionization efficiency data for the molecular ion and the two abundant low energy fragments of 2,2-difluoropropane are shown in Fig. 1. The onset of the molecular ion occurs at about 1086 Å, giving a value of 11.42 ± 0.02 eV for the adiabatic ionization potential of the parent neutral. The ionization efficiency rises with photon energy as more vibrational states of the ground state ion are populated, peaks at a photon energy slightly above the onset of the first fragmentation, and declines slightly for higher photon energies.

The major fragmentation pathways (1) and (2) account for

$$(CH_3)_2CF_2 \longrightarrow \begin{cases} CH_2CF_2^+ + CH_4 & (1) \\ CH_3CF_2^+ + CH_3 & (2) \end{cases}$$

the observed fragment ions. The $CH_2CF_2^+$ ion formed by loss of CH_4 from the molecular ion (process 1) exhibits an onset at 1072 ± 3 Å, corresponding to an appearance potential of 11.57±0.03 eV, and rises continually with photon energy above this point. The onset of the $CH_3CF_2^+$ cation, formed by loss of a methyl radical (process 2), occurs at 1050 ± 3 Å, or 11.81 ± 0.03 eV.

The thresholds observed in the present study are summarized in Table I. Also included in Table I are ion heats of formation derived from the measured threshold and from the thermochemical data for neutral species summarized in Table II.

Since the heat of formation of 2,2-difluoropropane is not available, the ΔH°_{f298} values quoted in Tables I and II for the parent

Figure 1

Photoionization efficiency curves for the molecular ion, $CH_2CF_2^+$, and $CH_3CF_2^+$ in 2, 2-difluoropropane.

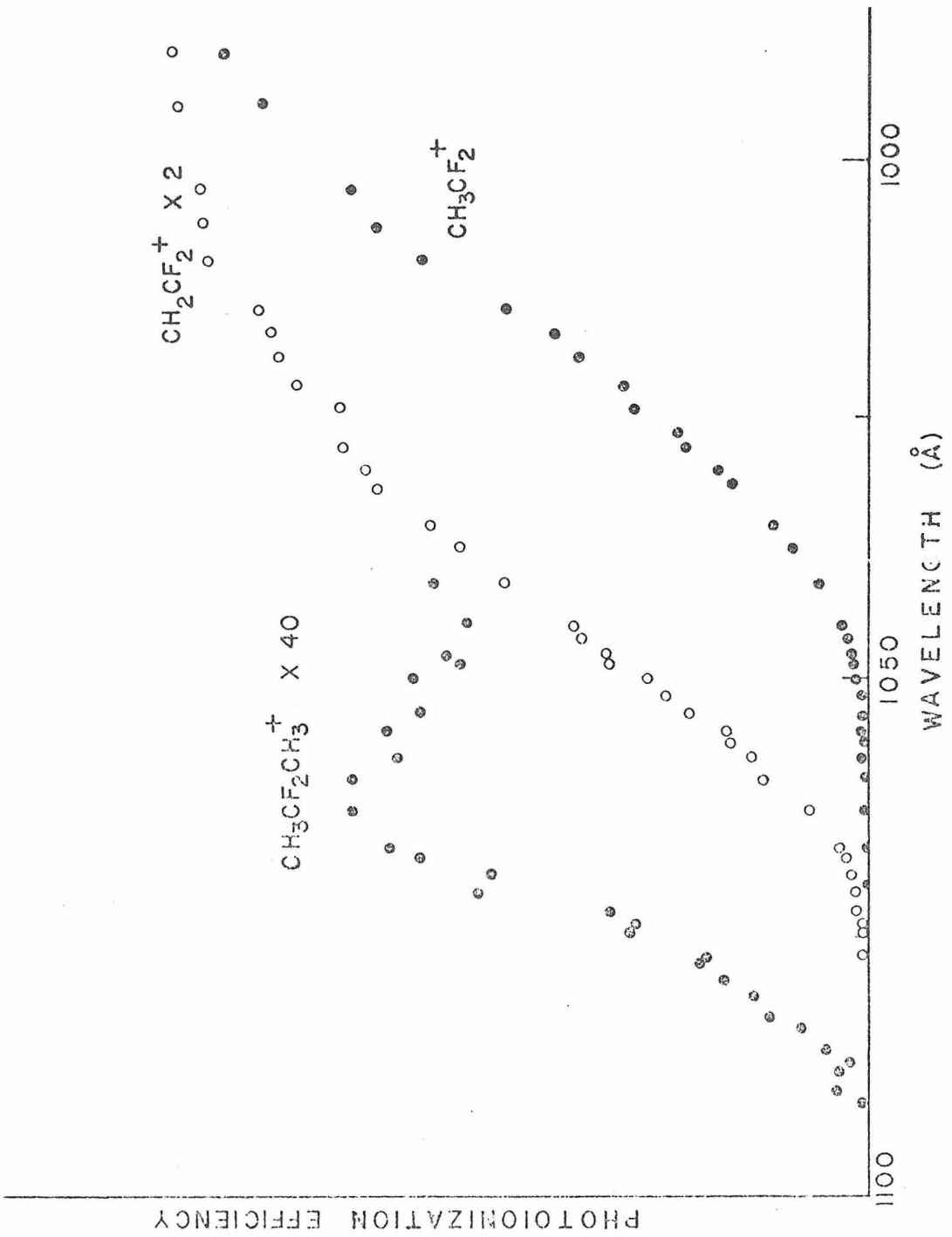
PHOTOIONIZATION EFFICIENCY
1100
1050
1000
WAVELENGTH (Å)
$CH_2CF_2^+$ X 2
$CH_3CF_2^+$
$CH_3CF_2CH_3^+$ X 40

Table I. Appearance Thresholds and Derived Heats of Formation

Molecule	Ion	AP or IP(eV)	$\Delta H^0_{f_{298}}$ (kcal/mole)
$(CH_3)_2CF_2$			-129.8 ± 3.0[a]
	$(CH_3)_2CF_2^+$	11.42 ± 0.02	133.5 ± 3.5
	$CH_2CF_2^+$	11.57 ± 0.03	154.8 ± 2.6[b]
	$CH_3CF_2^+$	11.81 ± 0.03	108.5 ± 3.2
$(CH_3)_2CHF$			-69.0 ± 1.0[b]
	$(CH_3)_2CHF^+$	11.08 ± 0.02	186.5 ± 1.5
	$(CH_3)_2CF^+$	11.23 ± 0.03	138.0 ± 1.7
	CH_2CHF^+	11.53 ± 0.03	214.9 ± 1.7[c]
	CH_3CHF^+	11.75 ± 0.03	168.0 ± 1.7[c]
CH_3CH_2F			-62.9 ± 0.4[b]
	CH_3CHF^+	12.04 ± 0.03	162.6 ± 1.1
CH_3CHF_2			-119.7 ± 1.5[b]
	$CH_3CF_2^+$	12.18 ± 0.03	109.1 ± 2.2

[a] Derived from thermochemical cycle using $\Delta H^0_{f_{298}}(CH_2CF_2^+)$.

[b] Table II.

[c] These values appear to be too high. There is a possibility that kinetic shift effects may be significant.

Table II. Selected Thermochemical Data

Compound		$\Delta H^{o}_{f_{298}}$
CH_3CH_2F		-62.9 ± 0.4[a]
CH_3CHF_2		-119.7 ± 1.5[a]
CH_3CF_3		-178.2 ± 0.4[a]
$(CH_3)_2CHF$		-69.0 ± 1.0[b]
$(CH_3)_2CF_2$		-129.8 ± 3.0[c]
CH_2CHF		-33.2 ± 0.4[d]
CH_2CF_2		-82.5 ± 2.4[e]
CH_3		34.0[f]
H		52.1[g]
IP(H)	=	13.598 eV[g]
$IP(CH_2CHF)$	=	10.36 ± 0.1 eV[h]
$IP(CH_2CF_2)$	=	10.29 ± 0.01 eV[h]

[a] S. S. Chen, A. S. Rodgers, J. Chao, R. S. Wilhoit, and B. J. Zwolinski, J. Phys. Chem. Ref. Data, 4, 441 (1975).

[b] J. R. Lacher, J. Phys. Chem., 60, 1454 (1956).

[c] Derived relative to $\Delta H^{o}_{f_{298}}(CH_2CF_2^+)$. See text for details.

[d] V. P. Kolesov and T. S. Papina, Russ. J. Phys. Chem., 44, 611 (1970). Corrected for the value of $\Delta H^{o}_{f_{298}}$ [HF, 40 H_2O] given in Ref. e.

[e] J. R. Lacher and H. A. Skinner, J. Chem. Soc., 1968A, 1034 (1968).

[f] J. A. Kerr, Chem. Rev., 66, 465 (1966).

[g] Ref. 20.

[h] Ref. 17.

molecule and its fragment ions are referenced to the value $\Delta H^{\circ}_{f298}(CH_2CF_2) = -82.5 \pm 2.4$ kcal/mole quoted in Table II. Using the ionization potential of CH_2CF_2 and the appearance potential of the $CH_2CF_2^+$ fragment ion in the present study, we assign the heat of formation of 2,2-difluoropropane to be -129.8 ± 3.5 kcal/mole. This value is consistent with an estimate of -125.8 kcal/mole obtained by the assumption that the contribution to the enthalpy of formation of replacing -H with $-CH_3$ is the same for CH_3CF_2H as for CH_3CH_3. The difference in the appearance potentials for processes (1) and (2) allow calculation of $\Delta H^{\circ}_{f298}(CH_3CF_2^+) = 108.5 \pm 3.5$ kcal/mole. In order to obtain an independent measurement of this value the appearance potential for this ion in CH_3CF_2H was measured to be 12.18 ± 0.04 eV, indicating a value of $\Delta H^{\circ}_{f298}(CH_3CF_2^+) = 10.90 \pm 1.2$ kcal/mole. The excellent agreement between the two values also gives further confidence in our assignment of the heat of formation for 2,2-difluoropropane as well as the published value for 1,1-difluoroethylene.

2-Fluoropropane

In 2-fluoropropane processes (3) - (5)

$$(CH_3)_2CHF \longrightarrow \begin{cases} (CH_3)_2CF^+ + H & (3) \\ CH_2CHF^+ + CH_4 & (4) \\ CH_3CHF^+ + CH_3 & (5) \end{cases}$$

were detected. Photoionization efficiency data for the parent ion and $(CH_3)_2CF^+$ fragment ion in 2-fluoropropane are shown in Fig. 2a. The threshold for ionization occurs at 1119 ± 2 Å, corres-

Figure 2

(a) Photoionization efficiency curves for the molecular ion and $(CH_3)_2CF^+$ fragment ion in 2-fluoropropane.

(b) Photoionization efficiency curves for $(CH_3)_2CF^+$, CH_2CHF^+, and CH_3CHF^+ fragment ions at lower magnification than (a).

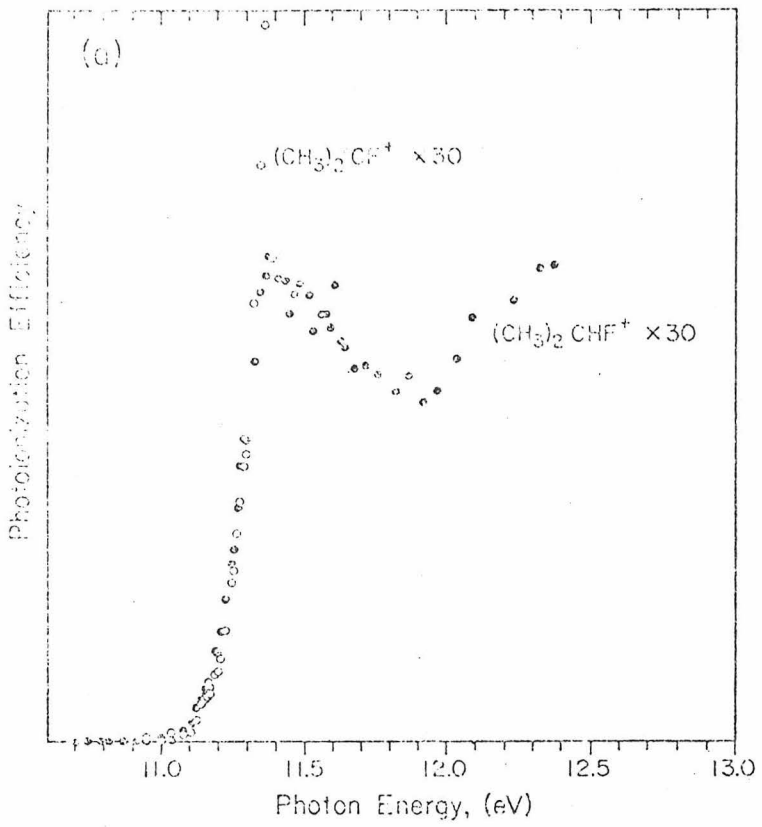
(a)
$(CH_3)_2 CF^+$ ×30
$(CH_3)_2 CHF^+$ ×30
Photoionization Efficiency
11.0
11.5
12.0
12.5
13.0
Photon Energy, (eV)

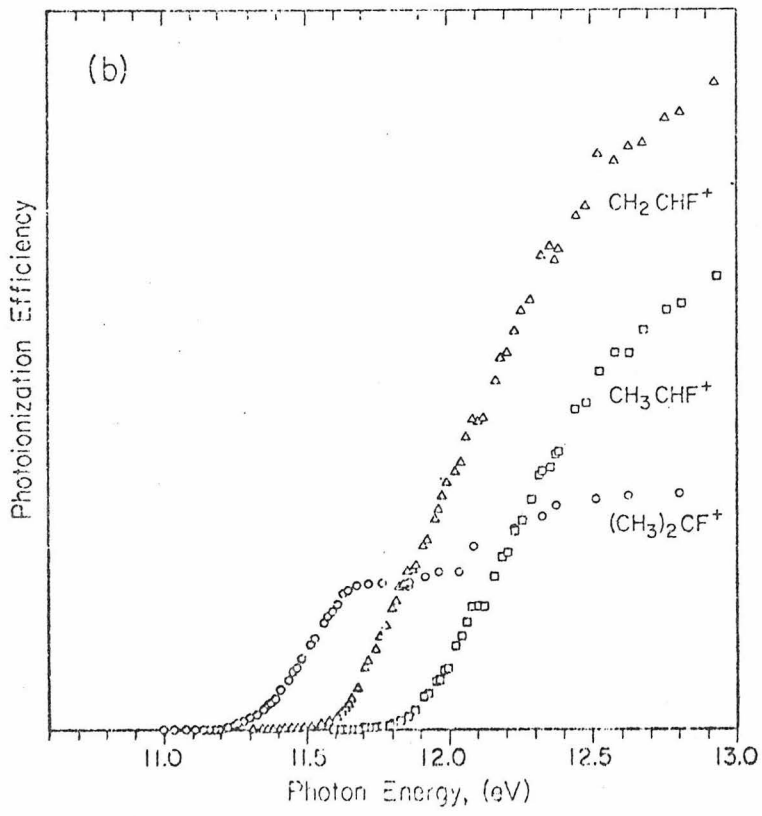
(b)
$CH_2 CHF^+$
$CH_3 CHF^+$
$(CH_3)_2 CF^+$
Photoionization Efficiency
11.0
11.5
12.0
12.5
13.0
Photon Energy, (eV)

ponding to an adiabatic ionization potential of 11.08 ± 0.02 eV. As in the 2,2-difluoropropane case, the parent curve reaches a maximum and declines as photon energy is increased. The $(CH_3)_2CF^+$ ion formed by process (3) shows an onset exactly coincident with the ionization potential. The ionization efficiency of the fragment essentially coincides with that of the parent ion from threshold to about 1095 Å, then continues to rise as the parent ion curve reaches a maximum. The behavior of the $(CH_3)_2CF^+$ ion is shown on a smaller magnification in Fig. 2b.

The appearance threshold of $(CH_3)_2CF^+$ is assigned as 1104 ± 3 Å (11.23 ± 0.03 eV), the wavelength at which the slopes of the parent and fragment ionization efficiency curve become equal. This point corresponds to the crossing point of the ion curves on a breakdown diagram[2]. This system is unusual in that the appearance potential for process (3) lies only 3.5 kcal/mole above the adiabatic ionization potential. Since the thermal vibrational energy distribution of the parent molecule at room temperature is expected to contain a significant population at energies greater than this difference, the onset of fragmentation coincides with the ionization potential. The threshold for process (3) allows calculation of the heat of formation of $(CH_3)_2CF^+$ to be 138.0 ± 1.0 kcal/mole. This number is consistent with the value of 143 ± 6 kcal/mole determined from limits set by ion-molecule reactions in 2-fluoropropane[16].

Figure 2b also shows the fragment ions of processes (4) and (5), analogous to the processes (1) and (2) in 2,2-difluoropropane. The apparent onset of process (4) is 1075 ± 3 Å (11.53 ± 0.03 eV),

and that for the α-cleavage process (5) is 1055 ± 3 Å (11.75 ± 0.03 eV). These thresholds would indicate heats of formation of 214.9 and 168.0 kcal/mole, respectively, for CH_2CHF^+ and CH_3CHF^+. The former value implies a heat of formation of vinyl fluoride of -24.0 kcal/mole, since the ionization potential of vinyl fluoride is well known[17]. There are indications that these values and thus the appearance potentials used to derive them may be too high. In particular, the literature contains various values for the heat of formation of vinyl fluoride[18-19], but the highest published number is -28 kcal/mole[20], and we favor the value of -33.2 ± 0.4 quoted in Table II.

As was done for the $CH_3CF_2^+$ ion, an independent study of the heat of formation of CH_3CHF^+ was performed by measuring the appearance potential of this ion from CH_3CH_2F. This appearance potential was found to be 12.04 ± 0.03 eV, yielding a value of 162.6 ± 1.0 kcal/mole for CH_3CHF^+. Thus the appearance potentials of both processes (4) and (5) appear to be too high. As discussed below, these findings are consistent with a significant kinetic shift for the two processes, or alternatively an error in the published heat of formation of 2-fluoropropane. As a result the derived heats of formation are quoted in Table I as upper limits to the true values.

Interestingly, neither 2-fluoropropane nor 2,2-difluoropropane exhibits a significant fragment ion resulting from the thermochemically favorable loss of HF from the molecular ion. In 2-fluoropropane, for example, this process has a computed threshold of 10.10 eV, which lies below the observed molecular ionization potential, yet the only ion observed at m/e 42 is clearly due to a propylene impurity

in the sample.

Proton Affinities of 1,1-Difluoroethylene and Vinyl Fluoride

The most abundant fragments in the fluorinated propanes in this study correspond to the molecular ions and protonated parent of the appropriate fluorinated ethylene. Since the difference in the thresholds for these fragmentations can be accurately measured, a thermodynamic cycle can be established which yields the proton affinities of the olefins, where proton affinity is defined as the negative enthalpy change on protonation as shown in equation (6). As mentioned above, proton affinity measurements on the fluoro-

$$B + H^+ \xrightarrow{\Delta H} BH^+ \qquad PA(B) = -\Delta H \qquad (6)$$

ethylenes provide independent determinations of the heats of formation of the fluorinated ethyl cations, so comparison of fragment appearance potential results with proton affinity measurements is desirable.

Table III summarizes a thermochemical cycle for both fluorinated propanes studied. As can be seen, the cycle yields the proton affinity for the relevant olefins using only the measured appearance potentials and well known thermochemical relationships. In particular, the heats of formation of neither the parent neutral nor the neutral fluoroethylene appear. The calculations of Table III give for 1,1-difluoroethylene a proton affinity of 174.8 ± 1.0 kcal/mole. For vinyl fluoride a proton affinity of 173.6 kcal/mole is computed, but error estimates are difficult to make in light of the uncertainty of the accuracy of the thresholds used.

Table III. Proton Affinities of CH_2CXF by Fragmentations of $(CH_3)_2CFX$ (X = F, H)

Process			ΔH(X = H)	ΔH(X = F)
$(CH_3)_2CFX$	→	$CH_3CFX^+ + CH_3$	271.0 kcal/mole	272.3 kcal/mole
$CH_4 + CH_2CFX^+$	→	$(CH_3)_2CFX$	-265.9	-266.8
CH_2CFX	→	CH_2CFX^+	238.9	237.3
$CH_3 + H$	→	CH_4	-104.0	-104.0
H^+	→	H	-313.6	-313.6
$CH_2CFX + H^+$	→	CH_3CFX^+	-173.6 kcal/mole	-174.8 kcal/mole

$PA(CH_2CHF)$ = 173.6 kcal/mole

$PA(CH_2CF_2)$ = 174.8 kcal/mole

Direct measurements of the proton affinities of the fluoroethylenes have been made by Ridge[9] using ion cyclotron resonance spectrometry. He finds that the proton affinity of 1,1-difluoroethylene is greater than that of ethyl iodide and less than that of methanol, assigning it a value of 177 ± 3 kcal/mole. Likewise he finds that vinyl fluoride has a proton affinity greater than water, less than formaldehyde, and approximately equal to hydrogen sulfide. Assigning these limits using an extensive tabulation of relative proton affinities[21] developed in our laboratories and those of Taft, we find the proton affinity of vinyl fluoride to be 171 ± 2 kcal/mole. The agreement between our data and the direct proton affinity measurements is excellent. In the case of 2-fluoropropane there seems to be a cancellation of errors in the difference of the thresholds used. It is interesting to note that if the heat of formation values of CH_2CHF taken from Table II is combined with the heat of formation of the proton and that of CH_3CHF^+ determined by H atom loss from CH_3CH_2F, a value of 171.9 kcal/mole is calculated for the proton affinity of vinyl fluoride.

Discussion

In evaluating the thresholds observed in this study attention must be paid to both the contribution of thermal internal energy of the neutral to the dissociation process and to the phenomenon of kinetic shift. These phenomena have been discussed in detail in the literature[22,23]. Since statistical theories of mass spectral fragmentations assume extensive randomization of internal energy

in the activated molecular ion, the initial thermal energy in the parent neutral is carried into the molecular ion where it contributes to the total internal energy there. This effect is expected to cause folding of a Maxwellian energy distribution into the threshold curve, causing a low energy "tail" on the fragment ionization efficiency curve and a shifting of the apparent threshold to lower energies by an amount equal to the mean thermal energy content of the parent molecule. These effects have been confirmed for fragmentations in the lower alkanes[23].

The second effect, that of kinetic shift, is defined as the displacement of the apparent thresholds to higher energies by the energy in excess of the fragmentation energy necessary to raise the fragmentation rate to the level at which the fragment ions can be detected. This effect is opposite in direction and often comparable in magnitude to the effect of thermal energy, leading to fortuitous cancellation of error. In our system the fragmentation rate k must be greater than 10^4 - 10^5 sec^{-1} to enable detection of the lowest energy fragment, an order of magnitude less than the rates necessary for detection on magnetic sector instruments. For fragmentations analogous to processes (1) and (3) in systems of similar size, kinetic shift effects have been calculated to be less than the quoted error of our thresholds[22].

For higher energy fragmentations the situation is quite different; decomposition rates must compete not only with the rate of extraction from the ion source but rather with the higher rate of fragmentation in the decomposition channel with lower threshold, and kinetic shifts

may be substantial.

Applying these principles to our systems sheds light on the interpretation of our data. The 2,2-difluoropropane fragmentations are typical of many systems in which the lowest energy fragmentation is a rearrangement process and the higher a simple bond fission. Here entropic factors strongly favor the "loose" intermediate of the higher energy process over the "tight" 4-center intermediate for the rearrangement. If this factor is great enough in the present system, the difference in kinetic shifts will be negligible and the relative thresholds will be accurate. One factor that suggests that matters may not be this simple is the continued rise of the $CH_2CF_2^+$ efficiency curve above the threshold for $CH_3CF_2^+$ production, suggesting that the two fragmentation rates are comparable over a large energy range. In any case the threshold for process (2) represents an upper bound. A lower bound can be determined from the fact that the CH_4 loss must be a lower energy process in order to compete with the α-cleavage. Using these considerations we can state with assurance that $0 < AP2 - AP1 \lesssim 0.24$ eV, resulting in the relationship 174.1 kcal/mole $\lesssim$ PA $(CH_2CF_2) <$ 179.6 kcal/mole. As mentioned above, the good consistency with other measurements indicates that the measured thresholds are not far wrong.

The 2-fluoropropane case is somewhat different in that both fragmentations (4) and (5) must compete with process (3), which has a very low threshold. The ionization efficiency curve for process (3) does stop rising abruptly slightly above the onset for process (4), indicating that the rate of fragmentation (4) is varying rapidly with

excess energy. However, the inconsistency of the heats of formation calculated from fragmentations (4) and (5) with those derived from other sources is bothersome. This difference can be attributed to a kinetic shift of about 7 - 9 kcal/mole in the thresholds of processes (4) and (5). In this event the cancellation of the kinetic shifts for the two thresholds to give a close estimate of the proton affinity must be considered fortuitous. Alternately, the possibility exists that the heat of formation of 2-fluoropropane is actually lower than the -69.0 kcal/mole quoted in Table II, as is suggested by recent flame calorimetry measurements of Kabo and Andreevskii[24].

References

1. B. Steiner, C. F. Giese, and M. A. Inghram, J. Chem. Phys., 34, 189 (1961).
2. W. A. Chupka and J. Berkowitz, J. Chem. Phys., 47, 2921 (1967).
3. E. Murad and M. A. Inghram, J. Chem. Phys., 40, 3263 (1964).
4. K. M. A. Refaey and W. A. Chupka, J. Chem. Phys., 48, 5205 (1968).
5. M. Krauss, J. A. Walker, and V. H. Dibeler, J. Res. N.B.S., 72A, 281 (1968).
6. T. B. McMahon, R. J. Blint, D. P. Ridge, and J. L. Beauchamp, J. Amer. Chem. Soc., 94, 8934 (1972).
7. R. J. Blint, T. B. McMahon, and J. L. Beauchamp, J. Amer. Chem. Soc., 96, 1269 (1974).
8. J. H. J. Dawson, W. A. Henderson, R. M. O'Malley, and K. R. Jennings, Int. J. Mass Spectrom. Ion Phys., 11, 61 (1973).
9. D. P. Ridge, J. Amer. Chem. Soc., 97, 0000 (1975).
10. J. Vogt and J. L. Beauchamp, submitted for publication.
11. S. A. Sullivan and J. L. Beauchamp, unpublished results.
12. S. A. Sullivan and J. L. Beauchamp, J. Amer. Chem. Soc., 97, 0000 (1975).
13. P. R. LeBreton, A. D. Williamson, J. L. Beauchamp, and W. T. Huntress, J. Chem. Phys., 62, 1623 (1975).
14. Chapters I and II, this thesis.
15. H. Morssan, Anal. Chim. Phys., 6, 19 (1890).

16. J. Y. Park and J. L. Beauchamp, unpublished results.

17. D. Reinke, R, Kraessig, and H. Baumgärtel, Z. Naturforsch, 28A, 1021 (1973).

18. In addition to the values quoted in Table II and Ref. 20, Benson (Ref. 19) predicts a value of -31.6 by group additivity methods.

19. S. W. Benson, Thermochemical Kinetics (Wiley, New York, N.Y., 1968).

20. J. L. Franklin, J. A. Dillard, H. M. Rosenstock, J. T. Herron, K. Draxl, and F. H. Field, Natl. Std. Ref. Data Ser., Natl. Bur. Std., No. 26 (1969).

21. J. F. Wolf, I. Koppel, R. W. Taft, R. H. Staley, and J. L. Beauchamp, unpublished results.

22. M. L. Vestal, "Ionic Fragmentation Processes," in Fundamental Processes in Radiation Chemistry, ed. P. Ausloos (Wiley, New York, N.Y., 1968).

23. W. A. Chupka, J. Chem. Phys., 54, 1936 (1971).

24. C. Y. Kabo and D. N. Andreevskii, Khim. Pronc., 43, 347 (1967).